Inorganic Chemistry

pubs.acs.org/IC

Article

Ligand Dictated Photosensitization of Iridium(III) Dithiocarbamate Complexes for Photodynamic Therapy

Monika Negi, Tejal Dixit, and V. Venkatesh*

Cite This: *Inorg. Chem.* 2023, 62, 20080−20095

Read Online

ACCESS | Metrics & More | Article Recommendations | Supporting Information

ABSTRACT: Organelle-targeted photosensitizers (PSs) for photodynamic therapy (PDT) are considered as an effective therapeutic strategy for the development of next generation PSs with the least side effects and high therapeutic efficacy. However, multiorganelle targeted PSs eliciting PDT via both type I and type II mechanisms are scarce. Herein, a series of cyclometalated iridium(III) complexes were formulated $[Ir(C\hat{}N)_2(S\hat{}S)]$ (C^N = 2-phenylpyridine (ppy) and 2-(thiophen-2-yl)pyridine (thpy); S^S = diethyldithiocarbamate (DEDTC), morpholine-*N*-dithiocarbamate (MORDTC) and methoxycarbonodithioate (MEDTC)) and the newly designed complexes Ir2@DEDTC and Ir1@MEDTC were characterized by single crystal X-ray crystallography. Complexes containing thpy as C^N ligand exhibit excellent photophysical properties such as red-shifted emission, high singlet oxygen quantum yield (ϕ_Δ) and longer photoluminescence lifetime when compared with complexes containing ppy ligands. Ir2@DEDTC exhibits the highest ϕ_Δ and photoluminescence lifetimes among the synthesized complexes. Therefore, Ir2@DEDTC was chosen to evaluate the photosensitizing ability to produce reactive oxygen species (ROS). Upon blue light irradiation (456 nm), it efficiently produces ROS, i.e., hydroxy radical ($^{\bullet}OH$) and singlet oxygen ($^1O_2$), which was confirmed by electron paramagnetic resonance (EPR) spectroscopy. *In vitro* photocytotoxicity toward HCT116, HeLa, and PC3 cell lines showed that out of all the synthesized complexes, Ir2@DEDTC has the highest photocytotoxic index (PI > 400) value. Ir2@DEDTC is efficiently taken up by the HCT116 cell line and accumulated mainly in the lysosome and mitochondria of the cells, and after PDT treatment, it elicits cell shrinkage, membrane blebbing, and DNA fragmentation. The phototherapeutic efficacy of Ir2@DEDTC has been investigated against 3D spheroids considering its ability to mimic some of the basic features of solid tumors. The morphology was drastically altered in the Ir2@DEDTC treated 3D spheroid after the light irradiation unleashed the potential of the Ir(III) dithiocarbamate complex as a superior PS for PDT. Hence, mitochondria and lysosome targeted photoactive cyclometalated Ir(III) dithiocarbamate complex exerting oxidative stress via both type I and type II PDT can be regarded as a dual-organelle targeted two-pronged approach for enhanced PDT.

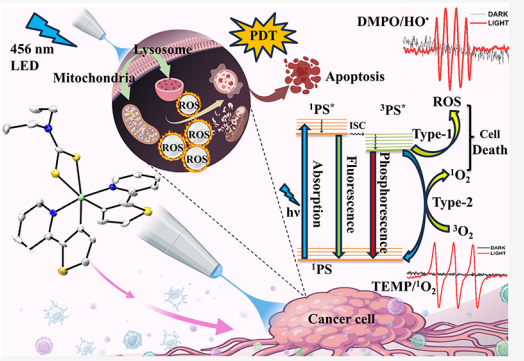

1. INTRODUCTION

Chemotherapy is one of the first-line medications for cancer treatment.[1] An increasing number of reports related to drug resistance and systematic toxicities resulted in the evolution of the field in search of new cancer treatment modalities. Light-activated therapy/phototherapy strategy has gained immense attention in the field of cancer treatment with improved therapeutic potential.[2,3] PDT is a light-mediated noninvasive anticancer strategy that involves a PS and a particular wavelength of light.[4] PDT works by two mechanisms: type I and type II.[5] In the case of type I PDT, PSs get activated with a specific wavelength of light which is accompanied by electron transfer to other biological substrates from the triplet excited state of PSs to produce ROS.[6] On the contrary, type II PDT involves interactions of the triplet excited state of PS with surrounding molecular triplet oxygen ($^3O_2$) upon light irradiation via energy transfer to generate cytotoxic $^1O_2$. These ROS are responsible for oxidative stress in cancer cells, which alters the redox homeostasis of cells and leads to irreversible cellular damage.[7] Hence, PDT has been extensively studied and considered as an effective cancer treatment strategy.

In recent years, various organic[8,9] and inorganic-based PSs have emerged as potent PS that can show excellent photophysical properties, e.g., long fluorescence lifetimes, large Stokes shifts, and high photostability.[10] In inorganic PSs, some organometallic cyclometalated iridium(III) complexes have already been addressed as potent candidates in the previous literature that has high $^1O_2$ production ability, giving them the potency to suppress cancer cells through type II

Received: August 23, 2023
Revised: November 2, 2023
Accepted: November 3, 2023
Published: November 23, 2023

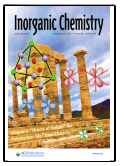

https://doi.org/10.1021/acs.inorgchem.3c02942
Inorg. Chem. 2023, 62, 20080−20095

PDT.[11−13] However, the clinical applications of many cyclometalated iridium(III) complexes are curtailed by their low quantum yield of $^1O_2$ production and short excited state lifetime.[14] Only a few iridium(III) cyclometalated complexes have been studied, which could show high ROS production by undergoing both type I[15,16] and type II PDT with long-lived triplet excited states.[17,18] Hence, there is a need for the development of PSs, which can be activated by both type I and II PDT for effective cancer therapy.

Additionally, PDT follows localized delivery of PSs and gets activated by specific light irradiation, which can diminish side effects on normal cells.[19] Because of its spatiotemporal specificity with the least side effects, the development of new and effective PSs can improve the therapeutic efficacy in the field of cancer treatment. Phosphorescent iridium(III) cyclometalated complexes have been widely reported to be able to localize at various cellular organelles, such as lysosomes,[20] mitochondria,[21−23] nuclei,[24−26] and endoplasmic reticulum.[27,28] A few studies have shown that some phosphorescent cyclometalated iridium(III) complexes accumulate in more than one organelle of the cell, such as lysosome and mitochondria,[29] nucleus and mitochondria,[30] etc., and show better therapeutic efficacy.

Neutral iridium(III) cyclometalated complexes with various ligands, such as imidoylamidinate,[31] β-diketonate,[32] and benzothiazole,[33] were reported as phosphorescence organic light-emitting diodes (OLEDs) as well as liquid droplet (LD)-specific[34] phosphorescent probes, respectively. Recently cationic-based Ir(III) cyclometalated complexes have been studied as glutathione sensing agents.[35] Also, neutral iridium(III) complexes bearing dithioformic acid ligands were reported as mitochondria-targeted cytotoxic agents.[36] However, the photophysical properties and their ability to act as PS for PDT have not been explored. Iridium(III) dithiocarbamate complexes also showed effective carbon disulfide (CS_2),[37] Hg^{2+} sensing,[38,39] as well as explored widely in the field of OLED.[40−42] However, these types of complexes are not well studied in terms of their cytotoxic applications.[43,44] Herein, we have chosen dithiocarbamate-based ligands for designing Ir(III) complexes because of the significant role of the sulfur atom as an efficient triplet harvesting unit.[45,46] Five neutral cyclometalated iridium(III) complexes, $[Ir(ppy)_2(DEDTC)]$ (Ir1@DEDTC, DEDTC = diethyldithiocarbamate), $[Ir(ppy)_2(MORDTC)]$ (Ir1@MORDTC, MORDTC = morpholine dithiocarbamate), $[Ir(ppy)_2(MEDTC)]$ (Ir1@MEDTC, MEDTC = methoxycarbonodithioate), $[Ir(thpy)_2(DEDTC)]$ (Ir2@DEDTC), and $[Ir(thpy)_2(MORDTC)]$ (Ir2@MORDTC), were synthesized. The potential complex Ir2@DEDTC was found to localize in mitochondria and lysosomes and exerts PDT via both type I and type II mechanisms. The structures of synthesized cyclometalated Ir(III) complexes are listed in Figure 1. The photophysical properties, cellular uptake, $^1O_2$ production, photocytotoxicity, and bioimaging applications were evaluated.

2. RESULTS AND DISCUSSION

2.1. Synthesis and Characterization. In this work, the investigated dithiocarbamate-based cyclometalated Ir(III) complexes were synthesized in two steps. First, The μ-chloride-bridged dimer Ir(III) complexes $[(ppy)_2\text{-Ir-}\mu\text{-Cl}]_2$ and $[(thpy)_2\text{-Ir-}\mu\text{-Cl}]_2$ were synthesized from iridium(III) chloride (precursor) using previously reported literature with minor modifications. Also, the potassium salt of morpholine

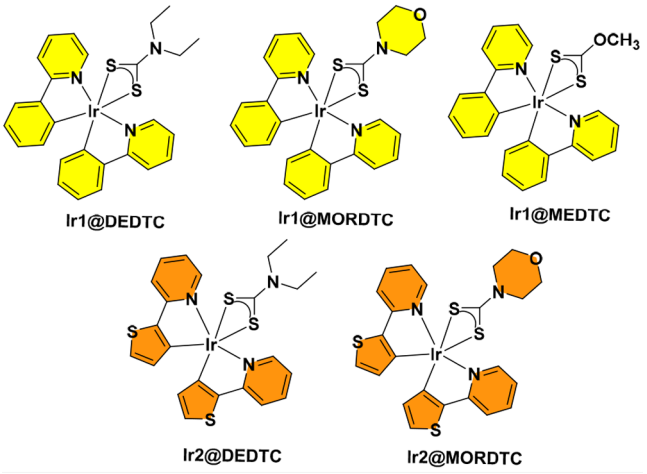

Figure 1. Molecular structures of synthesized cyclometalated Ir(III) complexes.

dithiocarbamate (MORDTC) and methoxycarbonodithioate (MEDTC) was prepared according to previously reported procedures, Scheme S1. Ir(III) dithiocarbamate complexes were synthesized by using $[(ppy)_2\text{-Ir-}\mu\text{-Cl}]_2$ and $[(thpy)_2\text{-Ir-}\mu\text{-Cl}]_2$ by following the synthetic route shown in Scheme 1. All

Scheme 1. Synthetic Route of Ir(III) Dithiocarbamate Complexes

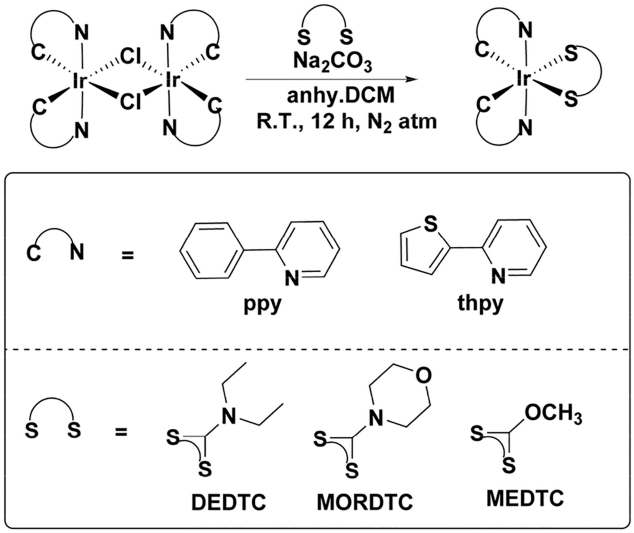

complexes are incorporated with one S^S ligand and two C^N ligands. We anticipate that incorporating sulfur in the form of $[(thpy)_2\text{-Ir-}\mu\text{-Cl}]_2$ dimer will enhance its photophysical properties, higher triplet excited state lifetime, photocytotoxicity, and cellular imaging ability of the complexes.[47] All the synthesized complexes were further characterized by ^{1}H NMR, ^{13}C NMR, and electrospray ionization (ESI-MS) spectroscopy (Figures S1−S21), as well as single crystal XRD.

2.1.1. X-ray Characterization. The single crystals of Ir1@MEDTC and Ir2@DEDTC suitable for X-ray diffraction (XRD) were crystallized by slow evaporation method with DCM-toluene (1:1, v/v) and ether diffusion method, respectively. The crystal structures of both Ir(III) complexes are shown in Figure 2. The complexes Ir1@MEDTC and Ir2@DEDTC were crystallized in monoclinic space groups $P2_1/n$

https://doi.org/10.1021/acs.inorgchem.3c02942
Inorg. Chem. 2023, 62, 20080−20095

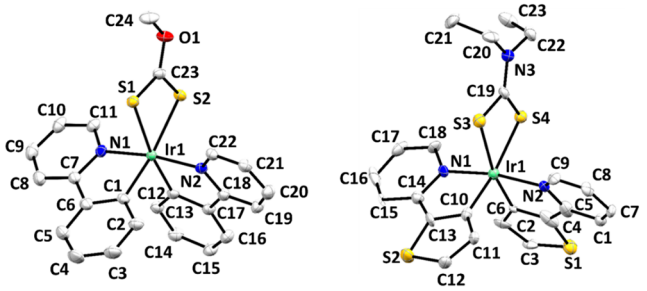

Figure 2. X-ray structures of complexes Ir1@MEDTC and Ir2@DEDTC (left to right).

and $P2_1/c$, respectively. The selected bond lengths in each complex are represented in Table S1. The details of single crystal data refinement parameters are summarized in Table S2.

2.2. Photophysical Properties. The UV−visible absorption spectra of all of the complexes in dry acetonitrile (CH_3CN) and DMSO−water (0.4%, v/v) at 298 K are shown in Figure 3(a) and Figure S22(a), respectively. The complexes display a strong absorption band in the region of 250−300 nm, which is assigned to spin-allowed ligand-centered or interligand ($^1\pi-\pi^*$) transitions.[48,49] In addition, the weak and broad absorption bands (less intense) in the region of 350−500 nm are designated to the mixed singlet and triplet metal-to-ligand charge transfer (MLCT) or dπ(Ir)−π^*-(L) (spin allowed and spin forbidden).[50,51] The absorption spectra for the synthesized Ir(III) complexes are analogous to most of the reported cyclometalated iridium(III) complexes.[52,53]

The fluorescence emission spectra for synthesized complexes were recorded in CH_3CN and DMSO-water (0.4%, v/v) at 298 K, are shown in Figure 3(b) and Figure S22(b). The emission maximum wavelengths of the synthesized Ir(III) complexes were almost the same in these solvents. The PL spectra of complexes Ir1@DEDTC, Ir1@MORDTC, and Ir1@MEDTC showed a broad green phosphorescent emission with maxima at 550 nm upon excitation at 405 nm. Moreover, complexes Ir2@DEDTC and Ir2@MORDTC showed an orange-red phosphorescent emission at 610 nm with a less intense narrow band at around 655 nm upon excitation at 450 nm. It is worth noting that these two complexes, i.e., Ir2@DEDTC and Ir2@MORDTC, exhibited a red-shifted (bathochromic) emission maxima of 100 nm compared to Ir1@DEDTC, Ir1@MORDTC, and Ir1@MEDTC complexes, suggesting the crucial role of different C^N ligands in modulating the photophysical properties. All of the complexes showed a minor solvatochromic effect and a large Stokes shift of about 150 nm. It has been extensively studied that a mixture of ^{3}MLCT and ligand-centered $^3(\pi-\pi^*)$ excited states is responsible for phosphorescence in iridium(III) cyclometalated complexes.[54] Moreover, all the synthesized complexes also showed excellent photostability as there was no visible change in the absorption peak under light irradiation (456 nm, 10 mW/cm^2) as well as under dark conditions for 48 h Figures S23 and S24. Excellent photostability is one of the important factors for a PS to generate ROS for hampering cancer cells. The photophysical properties of all of the synthesized

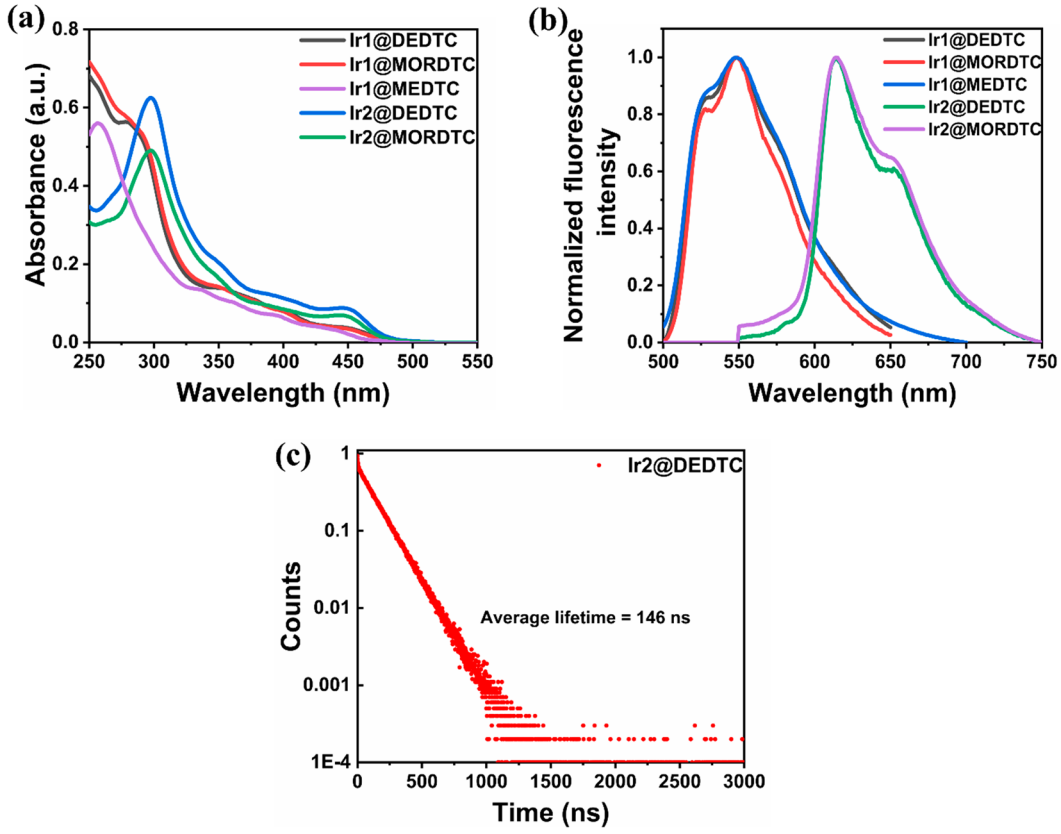

Figure 3. Absorption spectra (a) and emission spectra (b) of Ir(III) complexes (20 μM) recorded in CH_3CN at room temperature. (c) Fluorescence lifetime spectra of Ir2@DEDTC (Excitation pulse: 450 nm).

https://doi.org/10.1021/acs.inorgchem.3c02942
Inorg. Chem. 2023, 62, 20080−20095

iridium(III) complexes are illustrated in Table 1. The excellent photostability under light and dark conditions and longer absorption wavelength of complexes suggested that they could be used as effective PSs for PDT.

Table 1. Photophysical Properties of Ir(III) Dithiocarbamate Based Complexes

complex	λ_{exc}/nm	λ_{em}/nm	ϕ^{a}_{em}	$\phi(^1O_2)^{b}$	τ^{c}/ns
Ir1@DEDTC	405	550	0.107	0.281	1.3
Ir1@MORDTC	405	550	0.0046	0.239	2.18
Ir1@MEDTC	365	550	0.085	0.271	5.78
Ir2@DEDTC	450	610	0.025	0.864	146
Ir2@MORDTC	450	610	0.022	0.705	109

[a]Emission quantum yield considering $[Ru(bpy)_3]Cl_2$ as reference compound in deareated CH_3CN. [b]$^1O_2$ quantum yield in DMSO (MB as reference). [c]Average photoluminescence lifetime in aerated DMSO as solvent.

2.2.1. Lifetime Measurement. Most of the transition metal complexes comprise an intermediate lifetime of hundreds of ns to several μs because of mixed singlet−triplet states.[55] The average fluorescence lifetime of most of the Ir(III) complexes is a key factor in the production or generation of ROS, such as $^1O_2$.[56] For Type II PDT, a longer triplet excited-state lifetime is needed to transfer energy to the molecular oxygen. The inclusion of higher molecular weight atoms, such as sulfur, is attributed to spin−orbit coupling, which eventually leads to a longer triplet state lifetime.[57−59] Ir2@DEDTC showed a significantly longer fluorescence lifetime (146 ns) than Ir1@DEDTC (1.3 ns) Figure 3(c) and Figure S25 in aerated DMSO due to the incorporation of the sulfur atom in the C^N ligand. The sulfur-containing C^N ligands along with electron-rich S^S ancillary ligand facilitate better intersystem crossing due to smaller singlet−triplet energy gap. The enhanced triplet sensitization significantly influences the phosphorescence wavelength, excited state dynamics, and photosensitization abilities of Ir2@DEDTC and Ir2@MORDTC. It also exhibits a remarkably higher $^1O_2$ generation quantum yield, which indicates the phosphorescent emission nature of the complexes.

2.3. $^1O_2$ Production and Quantification. As iridium(III) complexes are prone to show type II photosensitization by quenching the triplet excited state with molecular oxygen to generate $^1O_2$, the ability of synthesized Ir(III) dithiocarbamate complexes to generate $^1O_2$ was studied with the help of 1,3-diphenylisobenzofuran (DPBF) as a $^1O_2$ scavenger in DMSO. Upon blue light irradiation, Ir(III) complexes produce $^1O_2$, which readily oxidizes DPBF to 1,2-dibenzoyl benzene (DBB). It resulted in the decrement of the DPBF absorbance peak maxima at 417 nm, which was used to quantify the production of $^1O_2$. The absorbance changes of DPBF alone with irradiation (456 nm) were recorded to show the degradation of DPBF without the complexes and reference compound. The absorbance of DPBF declined weakly after irradiation for 40 s due to the photobleaching of DPBF alone (Figure S26). Methylene blue (MB) is used as a reference PS while performing this assay. The absorbance maxima of DPBF decreases after the addition of PS with an increase in irradiation time.[60] Figure 4(a) shows a steady decrease in the absorption maxima of DPBF in the presence of Ir2@DEDTC under light irradiation after every 5 s. The values of ϕ_Δ for complexes were estimated by plotting the scatter plot for change in absorbance of DPBF for all complexes and

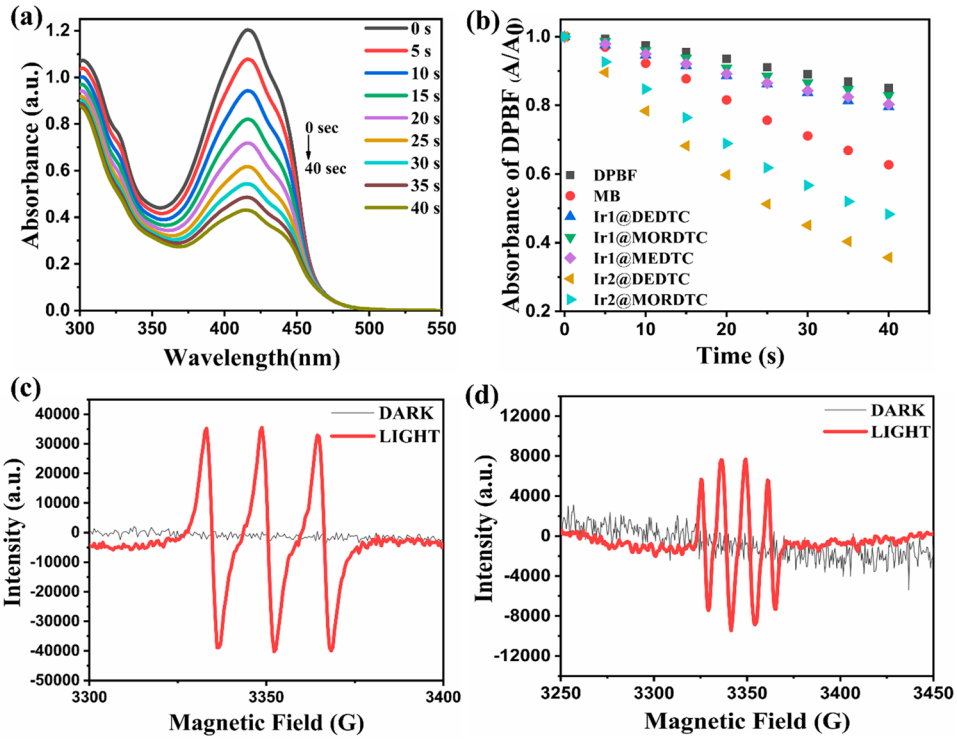

Figure 4. (a) Absorption changes of DPBF with Ir2@DEDTC after light irradiation (0−40 s). (b) Photooxidation of DPBF by complexes and the reference compound under light irradiation (450 nm, 10 mW/cm^2). (c) Ir2@DEDTC with TEMP in dark (gray line) and after 450 nm light irradiation for 20 min (red line). (d) Ir2@DEDTC with DMPO in dark (gray line) and after 450 nm light irradiation for 20 min (red line).

https://doi.org/10.1021/acs.inorgchem.3c02942
Inorg. Chem. 2023, 62, 20080−20095

Table 2. Photo-Cytotoxicities of Metal Complexes (μM) in Comparison to Cisplatin against HCT116 (Human Colorectal Carcinoma), HeLa (Human Cervical Carcinoma), and PC3 (Human Prostate Carcinoma) Cell Lines Expressed as Mean ± Standard Error (n = 3)

	HCT116			HeLa			PC3		
compound	dark	light[a]	PI[b]	dark	light[a]	PI[b]	dark	light[a]	PI[b]
Ir1@DEDTC	49.86 ± 3.10	1.75 ± 1.73	28	86.88 ± 4.2	22.73 ± 3.5	3.8	>100	>100	n.a.
Ir1@MORDTC	85.44 ± 3.28	4.51 ± 2.60	18.8	>100	50.88 ± 2.2	1.96	50.9 ± 6.2	45.3 ± 5.7	1.13
Ir1@MEDTC	39.88 ± 6.0	27.09 ± 7.4	1.5	>200	33.24 ± 1.8	6.02	90.04 ± 3.9	39.68 ± 5.2	2.3
Ir2@DEDTC	44.03 ± 5.83	0.1095 ± 1.2	>400	>300	4.12 ± 1.9	73	>100	58.91 ± 3.7	1.7
Ir2@MORDTC	25.98 ± 7.3	0.91 ± 2.3	28.6	>100	4.49 ± 2.7	22.3	>100	63.5 ± 4.7	1.59
Cis-Pt	20.77 ± 5.2	19.66 ± 6.3	1.05	17.64 ± 0.4.6	16.61 ± 4.1	1.06	10.5 ± 3.7	10.27 ± 2.9	1.02

[a]Irradiated at 456 nm LED light (30 mW/cm^2) for 40 min. [b]Photocytotoxicity index (PI = IC_{50}(dark)/ IC_{50}(light)) indicates the efficiency of the light treatment.

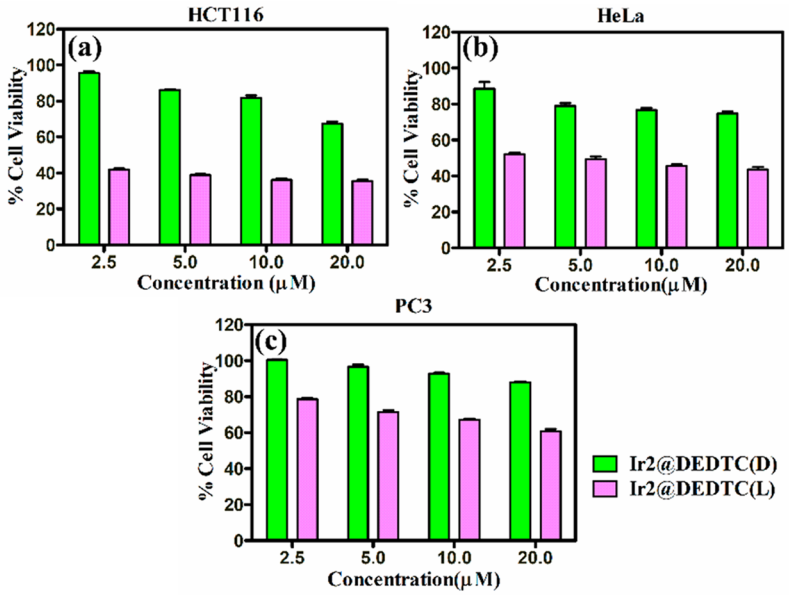

Figure 5. Cell viability was studied in HCT116(a), HeLa (b), and PC3 (c) cancer cells formulated with different concentrations of Ir2@DEDTC under dark and light conditions. Values are represented as the mean ± SD of three independent experiments.

reference compounds for different irradiation periods Figure 4(b). The results showed that the trend of the quantum yield for the generation of $^1O_2$ is as follows: Ir2@DEDTC (0.864) > Ir2@MORDTC (0.705) > Ir1@DEDTC (0.281) > Ir1@MEDTC (0.271) > Ir1@MORDTC (0.239). Herein, Ir2@DEDTC and Ir2@MORDTC showed significantly higher $^1O_2$ quantum yields than others, indicating that they could be efficient PSs. The UV−vis spectra of change in absorbance of DPBF with complexes with the thpy ligand showed a higher decline as compared to complexes containing ppy, suggesting a remarkable and rapid generation of ROS (Figure S26).

The ROSs generated by the triplet excited state PSs via the type I (electron transfer) or type II (energy transfer) pathway of PDT cannot be identified by EPR directly because of their short lifetimes. EPR is a sensitive and reliable technique to detect and identify the type of ROS with the help of spin-trapping agents such as 2,2,6,6-tetramethylpiperidine (TEMP) for $^1O_2$, 5,5-dimethyl-1-pyrroline *N*-oxide (DMPO) for other ROS species ($O_2^{\bullet-}$ and $^\bullet$OH) and 5-*tert*-butoxycarbonyl-5-methyl-1-pyrroline-*N*-oxide (BMPO) for $^\bullet$OH and thiyl (RS$^\bullet$) radical. The stable spin adducts, which are readily formed by reacting ROS with these diamagnetic spin traps, can be characterized and identified by EPR analysis. Herein, the EPR spin trapping technique is utilized to confirm further the ROSs generated by the complex Ir2@DEDTC. Upon irradiation with 450 nm light for 20 min, the deaerated CH_3CN solutions of Ir2@DEDTC (100 μM) and TEMP (50 mM), a three-line signal with equal intensities (1:1:1) emerged between 3300−3400 G magnetic field Figure 4(c). A hyperfine splitting constant of A = 15 G and a g factor of 2.0141 are observed for the TEMP/$^1O_2$ adduct. To verify the ability to generate other ROS by the Ir(III) complexes after light irradiation, we employed DMPO as the trapping agent for $O_2^{\bullet-}$ and $^\bullet$OH. Figure 4(d) represents a four-line spectrum, which is the characteristic spectrum of the DMPO/$^\bullet$OH adduct. Also, the generation of $^\bullet$OH is further confirmed by the BMPO/$^\bullet$OH adduct Figure S27. These results indicated that Ir2@DEDTC is capable of generating $^1O_2$ and $^\bullet$OH after irradiation with 450 nm light. The triplet excited state of a PS yields ROS only after light irradiation. No signals in EPR were observed in the dark (Ir2@DEDTC without light irradiation). The results indicated that synthesized complexes generate ROS after irradiation with 450 nm and could act as type I and type II PS.

2.4. *In Vitro* Photocytotoxicity and Cellular Uptake. After confirming that Ir(III) complexes undergo type I and type II photosensitization after light irradiation, we set out to investigate whether it could show photocytotoxicity against different cell lines by using cell viability assay (MTT assay).

https://doi.org/10.1021/acs.inorgchem.3c02942
Inorg. Chem. 2023, 62, 20080−20095

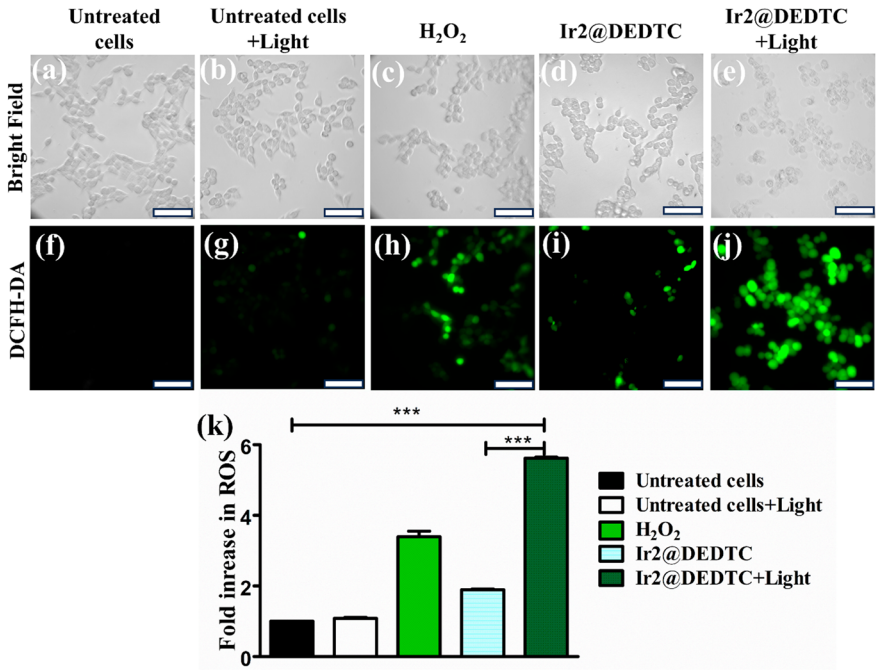

Figure 6. (a–e) Bright-field images of HCT116 captured after DCFH-DA staining. Cells alone without light, cells alone with light (456 nm, 30 mW/cm^2, 20 min), hydrogen peroxide (50 μM, positive control), Ir2@DEDTC (20 μM, without light), and Ir2@DEDTC (20 μM, with light) (left to right). (f–j) Corresponding fluorescence was obtained under the green channel. Magnification: 40×. Scale bar: 20 μm. (k) Quantitative statistical analysis of the production of ROS in the cells. Data expressed as mean ± SD (n = 2), p values were measured using one-way ANOVA with Turkey multiple comparison test, ***p < 0.001.

The IC_{50} (half-maximum inhibitory concentration) values with phototoxicity index (PI) values of synthesized complexes toward various cell lines are summarized in Table 2. Low dark toxicity was observed for HCT116, HeLa, and PC3 cells after 24 h of drug exposure and 24 h recovery. All the complexes were observed to be less toxic under dark conditions (IC_{50} = 44.03–85.44 μM). Upon light exposure, Ir2@DEDTC was found to be highly cytotoxic (IC_{50} = 0.1095 μM, PI > 400) against the HCT116 cell line by generating ROS. Complexes with thpy ligand, i.e., Ir2@DEDTC and Ir2@MORDTC, displayed higher cytotoxicity (lower IC_{50}) than cisplatin after light irradiation for 40 min against HCT116, HeLa cell lines as compared to PC3 cancer cell line. Additionally, Complexes also showed lower dark toxicity toward normal WRL-68 cell lines than dithiocarbamate (DTC) ligand alone Tables S3 and S4. Overall, our studies reflect the potential of Ir2@DEDTC and Ir2@MORDTC to act as potential PSs for PDT after irradiation with blue LED (456, 30 mW/cm^2 light) against HCT116 and HeLa cancer cell lines Figures 5 and S28. In contrast to the cytotoxicity studies of iridium(III) dithiocarbamate complexes reported previously,[36] in our experiment, we have noted that on the treatment of complexes for 24 h, followed by 24 h recovery, all the complexes exhibited poor dark toxicities (due to proliferation of cells during recovery period). It is also evident that the light induced cytotoxicities of the complexes are significant even after the recovery period. As Ir2@DEDTC has shown the maximum photocytotoxicity efficiency, it has been used as a lead molecule to carry out further investigations.

As the synthesized Ir(III) dithiocarbamate complexes showed better photocytotoxicities against HCT116 cell line, therefore the cellular uptake studies for Ir2@DEDTC were investigated in the same cell line using inductively coupled plasma mass spectrometry (ICP-MS). The amount of Ir(III) accumulated inside the cells (Ir content per 10^5 cells) is calculated with the help of standard graphs Figure S29. HCT116 cells were incubated with 20 μM Ir2@DEDTC with different incubation time intervals, i.e., 2, 4, 6, and 12 h. The result showed that intracellular Ir(III) content increases with increasing incubation time intervals, i.e., 2 h (131.6 nM Ir/10^5 cells) < 4 h (247.55 nM) < 6 h (249.9 nM) < 12 h (326.2 nM). To understand the selectivity of Ir2@DEDTC for HCT116 over PC3 cells, the uptake experiment was performed with PC3 cells. After 6 h of treatment, only 18.4 nM Ir/10^5 cells accumulated in PC3 cells, when compared with 249.9 nM Ir/10^5 cells accumulated in HCT116 cells (Table S5 and Figure S30). Hence, the lower uptake of complexes in the PC3 cell line could be the reason for the least dark toxicity and photocytotoxicity of the complexes.

2.5. Intracellular ROS Production (DCFH-DA Assay). ROS is an important factor in estimating PS-induced cytotoxicity after light irradiation. To detect the generation of ROS inside cells, a cellular ROS indicator, i.e., 2,7-dichlorodihydrofluorescein diacetate (DCFH-DA), is used to evaluate the ROS generation ability of Ir2@DEDTC in the HCT116 cell line in dark and light conditions with all the necessary control experiments. After cellular internalization, nonfluorescent DCFH-DA gets hydrolyzed to DCFH and further oxidized into a green fluorescent compound, i.e., dichlorofluorescein (DCF), in the presence of ROS.[61] HCT116 cells treated with Ir2@DEDTC, followed by 456 nm light irradiation, showed bright green fluorescence emission from cells Figure 6(j), which is better than that of the positive control (H_2O_2 treated cells) Figure 6(h), whereas, under dark conditions, green emission was observed from very few cells, Figure 6(i). Similarly, untreated cells with and

https://doi.org/10.1021/acs.inorgchem.3c02942
Inorg. Chem. 2023, 62, 20080–20095

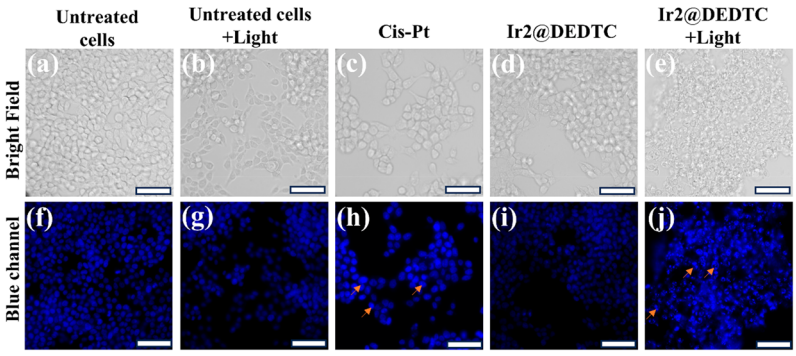

Figure 7. Nuclear fragmentation and chromatin condensation studies by DAPI staining. (a–e) Bright-field images obtained after DAPI staining for cells alone without light, cells alone with light (456 nm, 30 mW/cm^2, 20 min), Cisplatin (20 μM, positive control), Ir2@DEDTC (20 μM, without light), and Ir2@DEDTC (20 μM, with light) (left to right). (f–j) Corresponding fluorescence was obtained under the blue channel. Magnification: 40×. Scale bar: 20 μm. Arrows represent chromatin condensation and nucleus disintegration.

without light irradiation exhibit very weak fluorescence emission, Figure 6(f),(g). The fluorescence intensity of DCF (λ_{ex} = 485 nm, λ_{em} = 535 nm) is correlated with the fold increase in ROS production, which is measured by quantifying the fluorescence emission with the help of a microplate reader. Upon 20 min of light irradiation at 456 nm, the fluorescence intensity is increased about 6-fold in the presence of Ir2@DEDTC, indicating a large amount of ROS production in the cells as compared to untreated cells (Figure 6(k)). Therefore, these results signify that PDT-mediated ROS production is involved in apoptotic cell death caused by cyclometalated Ir(III) complex.

2.6. DNA Fragmentation Studies. Nuclear fragmentation study was performed by using 4′,6-diamidino-2-phenylindole (DAPI) to investigate the cause of cell death after light irradiation (456 nm, 30 mW/cm^2, 20 min). The cells in the control group (untreated cells with and without light) and Ir2@DEDTC without the light group showed no sign of DNA disintegration (chromatin condensation) Figure 7(f),(g),(i). Cisplatin (Cis-Pt) is used as a positive control, which shows some chromatin condensation with high fluorescence intensity for DAPI (Figure 7(h)). The morphological changes of the nucleus in the case of cells incubated with Ir2@DEDTC (20 μM) in the presence of light showed condensed chromatin and higher blue fluorescence intensity (Figure 7(j)). The presence of a greater extent of nuclear fragmentation in the Ir2@DEDTC+Light group, as compared to other groups, indicated that the cells were undergoing apoptosis through DNA damage.

2.7. Cell Morphology Change and Live/Dead Cell Staining. The apoptotic morphological changes, such as membrane blebbing, cellular fragmentation, and cell shrinkage, were investigated. The morphology of HCT116 cells in the control group (without Ir2@DEDTC treatment) showed insignificant changes with and without light conditions (Figure 8(a),(b)). No changes in morphology were observed in the case of HCT116 cells treated with Ir2@DEDTC under dark conditions (Figure 8(c)). On the other hand, most of the cell morphology has been dramatically changed after treatment with Ir2@DEDTC under light irradiation (456 nm, 30 mW/cm^2, 20 min, Figure 8(d)). This suggests that Ir2@DEDTC can efficiently induce cellular apoptosis under light irradiation.

To further verify the photocytotoxic profile of Ir2@DEDTC, fluorescein diacetate (FDA) and propidium iodide (PI) costaining assay was performed. Nonfluorescent FDA penetrates inside the viable cells easily and gets hydrolyzed into green emissive fluorescein by esterases present in the cytoplasm of live cells,[62] whereas PI is nonpermeable through the cell membrane and can intercalate with DNA for membrane-compromised cells (dead cells) and give red fluorescence after binding to DNA. In Figure 9(f),(g), most of the cells are viable (showing green fluorescence) in the case of untreated cells with and without light irradiation. Cells incubated with Ir2@DEDTC under dark conditions showed few dead cells and more live cells (Figure 9(r)). Upon irradiation with 456 nm light, the cells showed high red fluorescence of PI after 24 h as compared to 6 h of incubation with Ir2@DEDTC Figure 9(s),(t).

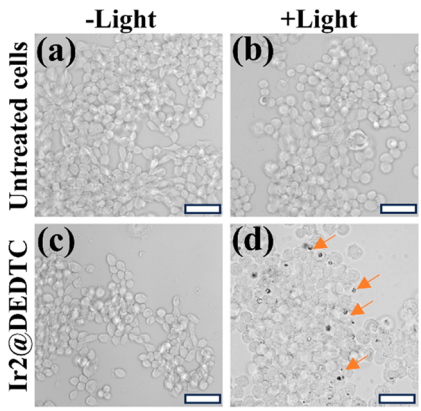

Figure 8. Morphology changes of HCT116 upon incubation with Ir2@DEDTC under light and dark conditions. Cells alone (a) without light and (b) with light (456 nm, 30 mW/cm^2, 20 min) and Ir2@DEDTC (20 μM) (c) with and (d) without light. Magnification: 40×. Scale bar: 20 μm. (Arrows represent cell shrinkage, membrane blebs, and rounding of cells).

2.8. Cellular Uptake and Intracellular Localization Studies. The cellular uptake of Ir2@DEDTC in HCT116 cells was visualized using fluorescence microscopy after 8 h of incubation (Figure S31). The intracellular colocalization of Ir2@DEDTC was investigated by colocalization assay in the presence of Mitotracker Green (Mitochondrial staining dye, MTG), Lysotracker Green (Lysosomal staining dye, LTG), and DAPI (nuclear stain) against HCT116 cell line. The merged images in Figure 10(d),(h) show the selective colocalization of MTG (Pearson's R value = 0.76) and LTG (R = 0.81) with complex Ir2@DEDTC. In contrast, costain

https://doi.org/10.1021/acs.inorgchem.3c02942
Inorg. Chem. 2023, 62, 20080−20095

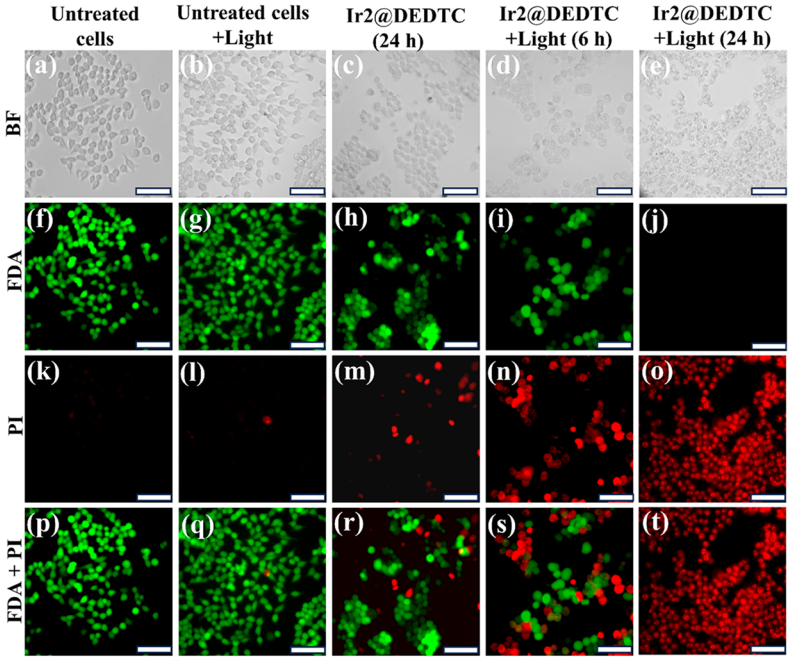

Figure 9. Live/dead costained HCT116 cells treated with Ir2@DEDTC for 6 and 24 h with or without light irradiation (456 nm, 30 mW cm^{-2}, 20 min). (a−e) Bright-field images of HCT116 captured after FDA/PI staining. Cells alone without light, cells alone with light, Ir2@DEDTC (20 μM, without light after 24 h), Ir2@DEDTC (20 μM, light irradiated after 6 h of incubation), and Ir2@DEDTC (20 μM, light irradiation after 24 h of incubation) (left to right). (f−j) Corresponding fluorescence was obtained under the green channel. (k−o) Corresponding fluorescence of PI was obtained under the red channel. (p−t) Merge images of green and red channels of the respective groups (green fluorescence: viable cells; red fluorescence: dead cells). Magnification: 40×. Scale bar: 20 μm.

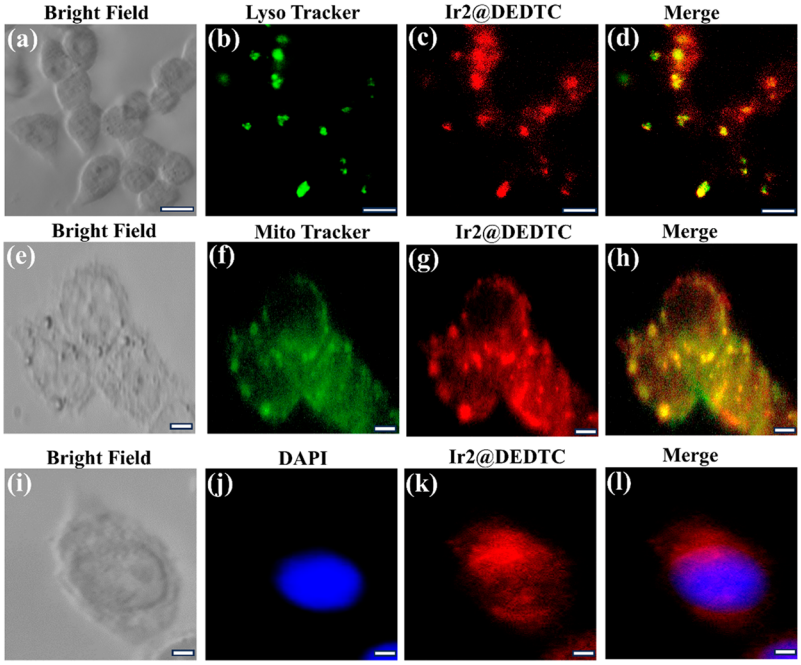

Figure 10. Colocalization assay with HCT116 cells incubated with Ir2@DEDTC costained with specific organelle targeting dye analyzed by fluorescence microscopy. (a−d) Bright-field, green channel (LTG), red channel (Ir2@DEDTC, 20 μM), and merged images of the cells incubated with Ir2@DEDTC (20 μM) and stained with LysoTracker Green (LTG, 500 nM) (left to right). scale bar: 10 μm. (e−h) Bright-field, green channel (MTG), red channel (Ir2@DEDTC, 20 μM), and merged images of the cells incubated with Ir2@DEDTC (20 μM) and stained with MitoTracker Green (MTG, 500 nM) (left to right). (i−l) Bright-field, blue channel, and red channel (Ir2@DEDTC, 20 μM) and stained with DAPI (1 μg/mL) (left to right). Magnification: 60× (DIC). Scale bar: 5 μm.

patterns of Ir2@DEDTC matched poorly with DAPI (Figure 10(l)).

Hence, we confirmed that Ir2@DEDTC was taken up effectively by the cells and predominantly localized in the lysosome and mitochondria of the cells. Also, the photo-

https://doi.org/10.1021/acs.inorgchem.3c02942
Inorg. Chem. 2023, 62, 20080−20095

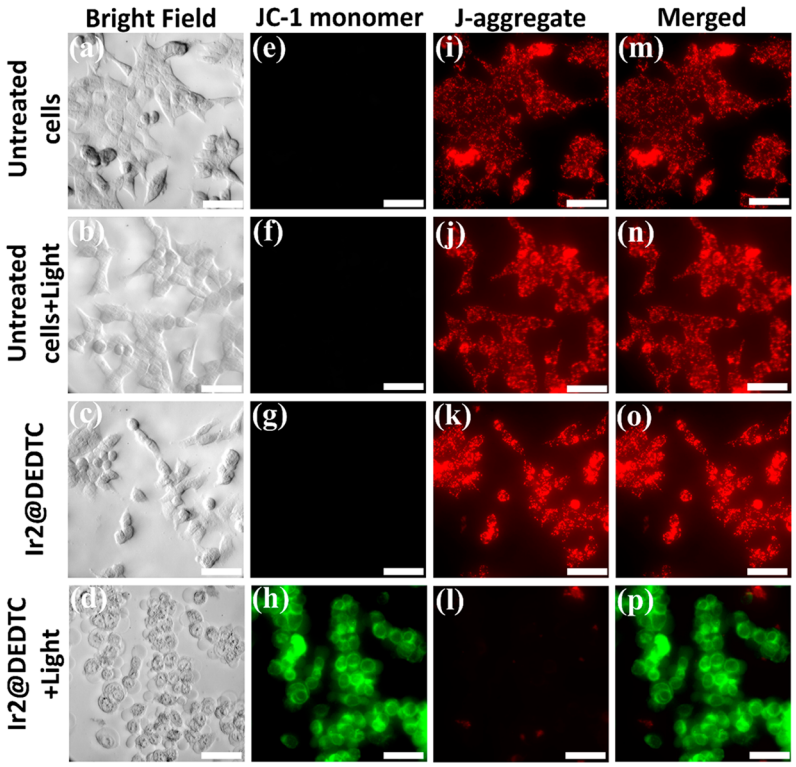

Figure 11. JC-1 stained HCT116 cells treated with Ir2@DEDTC for 6 h with or without light irradiation. (a–d) Bright-field images of HCT116 captured after JC-1 staining. Cells alone without light (a), cells alone with light (b), Ir2@DEDTC (20 μM, without light) (c), and Ir2@DEDTC (20 μM, with light) (d) (up to down). (e–h) Corresponding fluorescence of JC-1 monomer was obtained under the green channel. (i–l) Fluorescence of JC-1 aggregate was obtained under the red channel. (m–p) Merge images of green and red channels of the respective groups (green fluorescence: low MMP, red fluorescence: high MMP). Magnification: 40×. Scale bar: 20 μm.

cytotoxic behavior of the synthesized Ir(III) dithiocarbamate complexes may originate from lysosome and mitochondria-targeted cell death.

2.9. Induction of Cellular Apoptosis and Loss of Mitochondrial Membrane Potential (MMP). Based on the colocalization images by a fluorescence microscope, we further evaluated the impact of complex Ir2@DEDTC on mitochondrial membrane integrity in dark and light conditions against HCT116. Mitochondria dysfunction is an important hallmark of an intrinsic apoptotic pathway of the cell. 5,5′,6,6′-Tetrachloro-1,1′,3,3′-tetraethylimidacarbocyanine iodide (JC-1) is a fluorescent dye that forms J-aggregates and emits red fluorescence for intact and healthy mitochondria (high MMP). In contrast, JC-1 dye exists as a monomer and shows green fluorescence for mitochondria having a depolarized membrane (low MMP). In Figure 11, red fluorescence is observed for untreated cells under light and dark conditions. Also, Ir2@DEDTC, under dark conditions, showed red fluorescence, which depicts the mitochondrial integrity of the cells. In contrast, Ir2@DEDTC with light (456 nm, 30 mW/cm^2, 20 min) irradiation extensively showed green fluorescence corresponding to the JC-1 monomer. Hence, complex Ir2@DEDTC-treated cells are undergoing mitochondrion-mediated apoptosis by lowering the mitochondrial membrane potential.

The lowering of mitochondria membrane potential further suggested us to investigate the cell cycle disturbance by complex Ir2@DEDTC under dark and light conditions. The impact of Ir2@DEDTC on cell cycle distribution is evaluated with the help of a flow cytometer with propidium iodide (PI) staining. Figure 12 shows the distribution of cells in various phases (G0/G1, S, Sub G1, and G2/M) for untreated cells (a), Cisplatin as a positive control (b), and Ir2@DEDTC in dark (c) and light conditions (d) after 24 h. Figure 12(e) represents the bar graph representation of the distribution of the cells in all the phases. Cells in the Sub G1 phase correspond to apoptotic cells having fragmented DNA, which emits less fluorescence of PI. A prominent increase in the population of cells in Sub G1 phase is observed in the case of cells treated with Ir2@DEDTC for 24 h and then irradiated for 40 min. On the other hand, untreated cells and Ir2@DEDTC under dark conditions showed a lesser fraction of cells in Sub G1 phase, revealing that cells are undergoing an apoptotic phase after light irradiation. The fraction of cells in the G0/G1 phase is higher for Ir2@DEDTC+Light group as compared to other phases, and hence it reveals that the cells are undergoing cell cycle arrest at G0/G1 phase. On the other hand, Cisplatin treated cells (20 μM) showed cell cycle arrest in the G2M phase (Figure 12(e)). Interestingly, the high population of cells in G0/G1 for complex Ir2@DEDTC under light (30 mW/cm^2, 40 min) supports G0/G1 cell cycle arrest responsible for the high cytotoxicity of the synthesized Ir(III) complexes.

2.10. 3D Multicellular Tumor Spheroids Imaging. Based on the results obtained from photocytotoxicity assays in 2D monolayer cells, the potency of Ir2@DEDTC was evaluated against 3D multicellular tumor spheroids (MCTS) in the presence of light irradiation. To mimic the solid tumor environment, MCTS has appeared to be an *in vitro* model for evaluating the therapeutic potential of the drug. Like most solid tumors, MCTS shows a heterogeneous surrounding with a necrotic core at the center having hypoxic regions (oxygen

https://doi.org/10.1021/acs.inorgchem.3c02942
Inorg. Chem. 2023, 62, 20080–20095

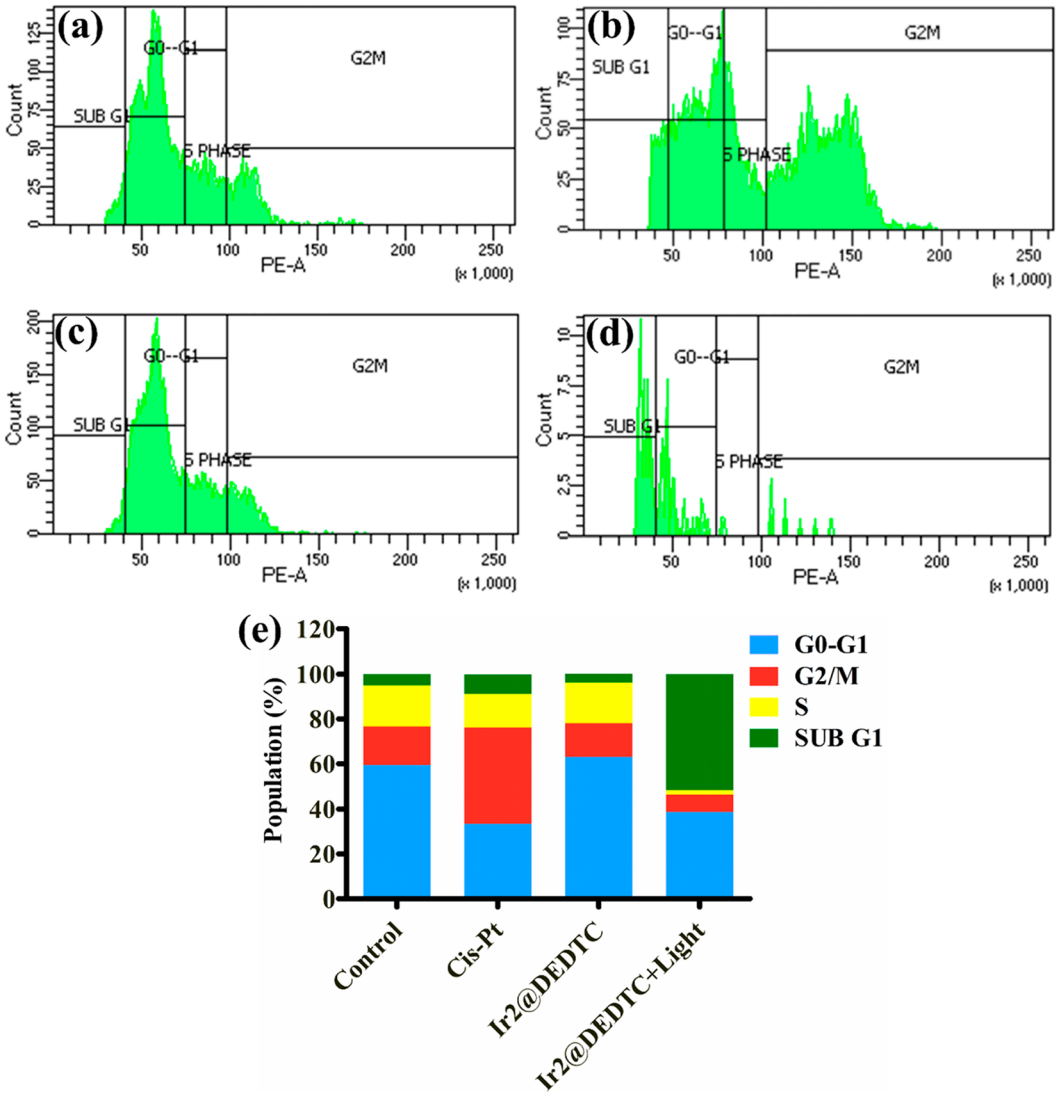

Figure 12. Flow cytometry analysis with PI staining in HCT116 cells treated with Ir2@DEDTC for 24 h with or without light irradiation. Cells alone (a), Cisplatin (b), Ir2@DEDTC (20 μM, without light) (c), and Ir2@DEDTC (20 μM, with light) (d). (e) Corresponding bar graph represents the cell population in G0/G1, Sub G1, S, and G2/M phases for all of the respective groups.

deficient).[63] Because of these factors, most of the drugs show great cytotoxicity on 2D monolayer cells but undergo drug resistance while performing *in vivo* studies. Hence, MCTS studies are the best model to show the therapeutic efficacy of the drug. The loss in the integrity of the spheroids was observed in Ir2@DEDTC after light irradiation when compared with the untreated spheroids as well as spheroid treated with Ir2@DEDTC under dark conditions Figure S32. These results indicated that a combination of Ir2@DEDTC and light showed cytotoxicity against MCTS.

To further investigate cell death in MCTS, a live/dead costaining assay was performed with the help of FDA and PI dye. The fluorescence images were captured in the green (for FDA) and red channels (for PI) after 24 h incubation with Ir2@DEDTC followed by light treatment. The Ir2@DEDTC +Light group showed fewer cells stained in the green channel when compared with other control groups. Also, the number of cells stained with PI in red channel was significantly higher in the Ir2@DEDTC+Light group as compared to untreated MCTS (CA and CA+Light) as well as Ir2@DEDTC under dark conditions (Figure 13). These results depicted that in the presence of light, Ir2@DEDTC exhibits potent photocytotoxicity in the MCTS model and induces cellular apoptosis.

CONCLUSIONS

In summary, we have synthesized a series of cyclometalated iridium(III) dithiocarbamate complexes with different C^N and S^S ligands. Out of the five synthesized complexes, two complexes, Ir2@DEDTC and Ir2@MORDTC, exhibited excellent photophysical properties such as red-shifted fluorescence emission, higher luminescence lifetime, and $^1O_2$ quantum yield. The role of ligands in dictating the photosensitizing ability of the complexes was evident from their photocytotoxicity assay. Ir2@DEDTC exhibits the highest photocytotoxic index against the HCT116 cell line and is found to be least toxic to normal human hepatic cells (WRL-68). Also, Ir2@DEDTC was efficiently taken up by HCT116 cells and predominantly localized in the lysosome and mitochondria. Furthermore, a combination of Ir2@DEDTC and light-induced apoptosis through lowering of the mitochondrial membrane potential and further induction of apoptosis was studied with JC-1 and cell cycle arrest analysis,

https://doi.org/10.1021/acs.inorgchem.3c02942
Inorg. Chem. 2023, 62, 20080−20095

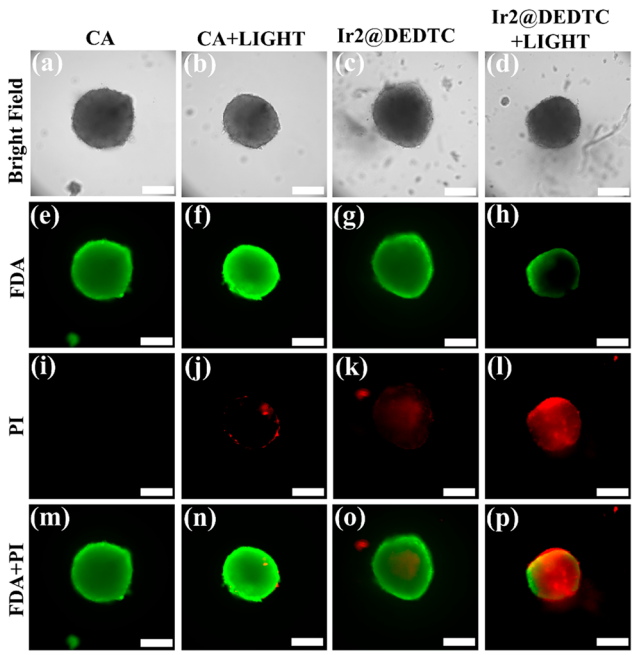

Figure 13. Live/dead costained HCT116 MCTS treated with Ir2@DEDTC, with and without light irradiation (456 nm, 30 mW cm^{-2}, 20 min). (a–d) Bright-field images of spheroids captured after FDA/PI staining. Cells alone (represented as CA) without light, cells alone with light, Ir2@DEDTC (20 μM, dark), and Ir2@DEDTC (20 μM, light irradiated after 24 h incubation) (left to right). (e–h) Corresponding fluorescence was obtained under the green channel. (i–l) Corresponding fluorescence of PI was obtained under the red channel. (m–p) Merge images of green and red channels of the respective groups. Magnification: 10×. Scale bar: 100 μm.

respectively. Finally, the photosensitization ability of Ir2@DEDTC was evaluated against the solid tumor mimicking 3D multicellular spheroid model and found efficient in destructing the 3D spheroids via type I and type II PDT.

4. EXPERIMENTAL SECTION

4.1. Materials and Methods. *4.1.1. Materials.* All starting materials and reagents were obtained from commercial distributors and used in the synthesis as obtained. Iridium(III)chloride hydrate ($IrCl_3 \cdot xH_2O$), LysoTracker Green DND-26, and MitoTracker Green FM were obtained from Thermo Fisher Scientific. 2-(Thiophen-2-yl)pyridine was purchased from BLD Pharma India. Sodium diethyldithiocarbamate and morpholine were purchased from AVRA. DAPI, DPBF, and DCFH-DA were purchased from Sigma-Aldrich. Deuterated solvents such as DMSO-d_6 and $CDCl_3$ were purchased from Eurisotop. Deionized water is used to perform all the experiments wherever required. The remaining chemicals were all of analytical grade and obtained from commercial sources.

4.1.2. Instruments. Nuclear magnetic resonance spectra (NMR) were recorded on a JEOL-500 MHz spectrometer (^{1}H NMR: 500 MHz, ^{13}C NMR: 126 MHz). UV–visible absorption data were acquired on a Shimadzu UV-2600 UV/vis/NIR spectrophotometer. The emission spectra were recorded with a Horiba Fluoromax. The fluorescence lifetimes for synthesized Ir(III) complexes were measured with the help of an Edinburgh FLS 1000 (TCSPC) spectrometer. The cell viability assays were performed with the help of a SYNERGY H1 microplate reader. The irradiation process during photocytotoxicity determination was conducted with the help of photoreactor Luzchem EXPO-01 panels with blue LED (456 nm).

4.1.3. Cell Lines and Culture Maintenance. HeLa (human cervical cancer) and HCT116 (human colon cancer), human hepatic cells (WRL-68), and PC3 (human prostate cancer) cell lines were purchased from the National Centre for Cell Science (NCCS), Pune, Maharashtra, India. Dulbecco's modified Eagle's medium (DMEM) along with 10% fetal bovine serum (FBS), 2.2 g/L sodium bicarbonate, streptomycin (100 mg/mL) and penicillin G (100 units/mL) is used to grow the cells. Fetal bovine serum (FBS) was purchased from Gibco (Thermo Fisher Scientific). All the cell lines were cultured at approximately 70–80% confluence and kept in a humidified incubator at 37 °C with 5% CO_2 in cell culture flasks with different sizes or plates (tissue cultured), depending on the type of experiments to be performed.

4.2. Synthesis of Ir(III) Complexes. *4.2.1. Synthesis of $[(ppy)_2$-Ir-μ-Cl$]_2$ Dimer.* Iridium dimer $[(ppy)_2$-Ir-μ-Cl$]_2$ is synthesized by previously reported literature with minor modifications.[64] Briefly, iridium(III) chloride (100 mg, 0.275 mmol, 1 equiv) hydrate was suspended in 2-ethoxyethanol/water (3:1), and 2-phenylpyridine (107 mg, 0.68 mmol, 2.5 equiv) was added. The reaction mixture was refluxed overnight to obtain a yellow precipitate. The formed precipitate was filtered and then washed several times with ethanol and further with diethyl ether to get a bright yellow solid (yield 61%). ^{1}H NMR (500 MHz, DMSO-d_6) δ 9.81 (d, J = 5.1 Hz, 2H), 9.53 (d, J = 4.9 Hz, 2H), 8.26 (d, J = 8.0 Hz, 2H), 8.18 (d, J = 7.7 Hz, 2H), 8.10 (t, J = 7.0 Hz, 2H), 8.01 (t, J = 7.0 Hz, 2H), 7.79 (d, J = 6.7 Hz, 2H), 7.73 (d, J = 6.9 Hz, 2H), 7.57 (t, J = 6.0 Hz, 2H), 7.45 (t, J = 5.9 Hz, 2H), 6.90 (t, J = 6.9 Hz, 2H), 6.84 (t, J = 6.9 Hz, 2H), 6.77 (t, J = 6.8 Hz, 2H), 6.69 (t, J = 6.8 Hz, 2H), 6.25 (d, J = 6.8 Hz, 2H), 5.66 (d, J = 6.9 Hz, 2H). ^{13}C NMR (126 MHz, DMSO-d_6) δ 167.36, 167.00, 152.14, 152.09, 150.68, 145.41, 143.80, 143.22, 139.26, 138.20, 131.29, 129.97, 129.69, 129.01, 124.86, 123.86, 123.62, 122.89, 122.31, 122.02, 120.13, 119.50.

4.2.2. Synthesis of MORDTC. The potassium salt of morpholine dithiocarbamate was prepared by already reported literature with minor modifications.[65] Morpholine (500 mg, 5.7 mmol, 1 equiv) and KOH (322 mg, 5.7 mmol, 1 equiv) were suspended in 5 mL of ethanol, and the reaction mixture temperature was maintained at 0 °C. After that, 200 μL of carbon disulfide (CS_2) was added until the solution color changed to light yellow and stirred vigorously for 1 h to get a white precipitate. Then it was washed with cold diethyl ether and dried under a vacuum to get the product as a white solid. (Yield 86%). ^{1}H NMR (500 MHz, DMSO-d_6) δ 4.33–4.27 (m, 4H), 3.52–3.46 (m, 4H).^{13}C NMR (126 MHz, DMSO-d_6) δ 215.04, 66.68, 50.11.

4.2.3. Synthesis of $[(thpy)_2$-Ir-μ-Cl$]_2$. $[(thpy)_2$-Ir-μ-Cl$]_2$ is synthesized according to the previously reported literature with slight modifications.[66] Iridium(III) chloride (100 mg, 0.275 mmol, 1 equiv) hydrate was dissolved in 2-ethoxyethanol/water (3:1), and 2-(thiophen-2-yl)pyridine (107 mg, 0.68 mmol, 2.5 equiv) was added. The reaction mixture was then allowed to reflux overnight to give a brown precipitate. The precipitate was filtered and simultaneously washed with ethanol and diethyl ether several times to obtain a reddish-brown solid (yield 65%). ^{1}H NMR (500 MHz, DMSO-d_6) δ 9.63 (d, J = 5.5 Hz, 2H), 9.31 (d, J = 5.4 Hz, 2H), 7.96 (t, J = 7.8 Hz, 2H), 7.89 (t, J = 7.7 Hz, 2H), 7.75 (d, J = 7.9 Hz, 2H), 7.63 (d, J = 7.7 Hz, 2H), 7.52 (d, J = 4.8 Hz, 2H), 7.36 (dd, J = 10.3, 4.3 Hz, 2H), 7.32 (d, J = 4.8 Hz, 2H), 7.23 (t, J = 7.4 Hz, 2H), 6.12 (d, J = 4.8 Hz, 2H), 5.66 (d, J = 4.8 Hz, 2H). ^{13}C NMR (126 MHz, DMSO-d_6) δ 163.44, 163.00, 154.08, 152.40, 150.94, 146.53, 139.81, 138.92, 136.44, 135.85, 130.72, 129.42, 128.29, 120.67, 120.23, 118.36, 118.11.

4.2.4. General Procedure for the Synthesis of Iridium(III) Complexes. Iridium dimer (50 mg, 1 equiv) was dissolved in dry DCM, and dithiocarbamate ligand (5 equiv) and Na_2CO_3 (10 equiv) were slowly added into the solution. The reaction mixture is then stirred at room temperature overnight under an inert atmosphere. After reaction completion (confirmed by TLC), the solvent was evaporated under reduced pressure on the rotary evaporator. The aqueous layer was further extracted by DCM, dried over sodium sulfate, concentrated under reduced pressure, and then purified using silica gel column chromatography (1:9 ethyl acetate/hexane).

4.2.4.1. Complex Ir1@DEDTC. Yellowish green solid (Yield 75%). ^{1}H NMR (500 MHz, $CDCl_3$) δ 9.63 (dd, J = 6.2, 1.1 Hz, 2H), 7.86

https://doi.org/10.1021/acs.inorgchem.3c02942
Inorg. Chem. 2023, 62, 20080–20095

(d, J = 7.8 Hz, 2H), 7.75−7.69 (m, 2H), 7.56 (dd, J = 7.7, 1.3 Hz, 2H), 7.20 (ddd, J = 7.3, 5.8, 1.5 Hz, 2H), 6.80−6.75 (m, 2H), 6.67 (td, J = 7.4, 1.3 Hz, 2H), 6.34 (dd, J = 7.8, 1.0 Hz, 2H), 3.77 (dd, J = 13.7, 7.0 Hz, 2H), 3.53 (dd, J = 13.7, 7.0 Hz, 2H), 1.23 (t, J = 7.1 Hz, 6H). ^{13}C NMR (126 MHz, $CDCl_3$) δ 211.10, 168.82, 155.90, 151.56, 144.03, 135.88, 131.51, 128.85, 123.84, 122.07, 120.71, 118.44, 43.65, 12.43. HRMS (ESI): calculated for $C_{27}H_{27}IrN_3S_2$ m/z 650.1276; found m/z 650.1233 $[M + H]^+$.

4.2.4.2. Complex Ir1@MORDTC. Yellowish green solid (Yield 78%). ^{1}H NMR (500 MHz, $CDCl_3$) δ 9.56−9.52 (m, 2H), 7.87 (d, J = 8.4 Hz, 2H), 7.77−7.71 (m, 2H), 7.56 (d, J = 8.1 Hz, 2H), 7.21 (t, J = 6.6 Hz, 2H), 6.80 (t, J = 6.9 Hz, 2H), 6.68 (t, J = 6.8 Hz, 2H), 6.32 (d, J = 8.7 Hz, 2H), 3.92−3.89 (m, 2H), 3.85−3.81 (m, 2H), 3.70 (t, J = 4.7 Hz, 4H). ^{13}C NMR (126 MHz, $CDCl_3$) δ 213.15, 168.71, 154.91, 151.54, 143.99, 136.10, 131.51, 128.96, 123.89, 122.22, 120.91, 118.52, 66.10, 46.18. HRMS (ESI): calculated for $C_{27}H_{25}IrN_3OS_2$ 664.1068 m/z; found m/z 685.4500 $[M + Na]^+$.

4.2.4.3. Complex Ir1@MEDTC. Yellowish green solid (Yield 72%) ^{1}H NMR (500 MHz, DMSO-d_6) δ 9.19 (d, J = 5.8 Hz, 2H), 8.20 (d, J = 7.9 Hz, 2H), 7.99 (td, J = 8.1, 1.5 Hz, 2H), 7.76 (d, J = 8.8 Hz, 2H), 7.47 (t, J = 6.6 Hz, 2H), 6.81 (t, J = 8.0 Hz, 2H), 6.67 (t, J = 8.0 Hz, 2H), 6.16 (d, J = 8.5 Hz, 2H), 4.08 (s, 3H). ^{13}C NMR (126 MHz, DMSO-d_6) δ 232.57, 167.84, 152.23, 151.63, 144.55, 138.09, 131.27, 129.31, 124.85, 123.92, 121.66, 119.72, 58.23. HRMS (ESI): calculated for $C_{24}H_{20}IrN_2OS_2$ m/z 609.0646; found m/z 609.0617 $[M + H]^+$.

4.2.4.4. Complex Ir2@DEDTC. Bright orange solid (yield 76%). ^{1}H NMR (500 MHz, $CDCl_3$) δ 9.40 (dd, J = 6.4, 2.1 Hz, 2H), 7.59 (ddd, J = 8.1, 7.4, 1.6 Hz, 2H), 7.48 (ddd, J = 8.1, 1.6, 0.9 Hz, 2H), 7.12 (d, J = 4.8 Hz, 2H), 6.98 (ddd, J = 7.5, 5.9, 1.6 Hz, 2H), 6.21 (d, J = 4.8 Hz, 2H), 3.75 (dd, J = 14.0, 7.2 Hz, 2H), 3.52 (dd, J = 13.9, 7.2 Hz, 2H), 1.23 (t, J = 7.2 Hz, 6H). ^{13}C NMR (126 MHz, $CDCl_3$) δ 210.76, 165.20, 157.32, 151.98, 136.32, 135.74, 131.13, 127.61, 118.83, 117.22, 43.51, 12.41. HRMS (ESI): calculated for $C_{23}H_{23}IrN_3S_4$ m/z 662.0404; found m/z 662.0359 $[M + H]^+$.

4.2.4.5. Complex Ir2@MORDTC. Bright orange solid (yield 65%). ^{1}H NMR (500 MHz, $CDCl_3$) δ 9.32 (d, J = 5.8 Hz, 2H), 7.64−7.58 (m, 2H), 7.49 (d, J = 8.5 Hz, 2H), 7.14 (d, J = 4.7 Hz, 2H), 7.00 (ddd, J = 7.4, 5.9, 1.5 Hz, 2H), 6.20 (d, J = 4.7 Hz, 2H), 3.89 (dd, J = 10.9, 5.2 Hz, 4H), 3.70 (t, J = 4.9 Hz, 4H). ^{13}C NMR (500 MHz, $CDCl_3$) δ 212.79, 165.09, 156.31, 151.98, 136.54, 135.82, 131.04, 127.75, 119.01, 117.30, 66.04, 46.00. HRMS (ESI): calculated for $C_{23}H_{21}IrN_3OS_4$ m/z 676.0197; found m/z 676.0150 $[M + H]^+$.

4.3. Quantification of $^1O_2$ Generation (ϕ_Δ). $^1O_2$ was quantified using UV−vis absorbance spectroscopy with DPBF as an indicator.[67] DPBF assay was performed according to previously reported literature.[68] The quantum yields of $^1O_2$ production in the presence of synthesized Ir(III) complexes after photoirradiation were calculated with the help of degradation of the absorbance of DPBF (417 nm). Briefly, a 50 μM solution of DPBF (alone) in DMSO is prepared, and the absorbance at 417 nm every 5 s after irradiation with a 456 nm (10 mW/cm^2) light source was recorded. DMSO solution of Ir(III) complex (20 μM) and DPBF (50 μM) were prepared in the dark conditions and then irradiated at 456 nm with the same light source. Further, the absorbance spectra of DPBF at 417 nm were recorded from 5 to 40 s of irradiation. Methylene blue (MB) was taken as a reference control ($\phi_{\Delta(DMSO)}$ = 0.52). The absorbances of the complex and methylene blue are kept constant at 456 nm. The formula to calculate the quantum yield of $^1O_2$ is as follows:

$$\phi_{\Delta(unk)} = \phi_{\Delta(MB)} \times (m_{(unk)} \times F_{(MB)})/(m_{(MB)} \times F_{(unk)})$$

where ϕ denotes $^1O_2$ quantum yield, m represents the slope of the graph between absorbance changes with time, and F is the correction factor for absorption.

4.4. Fluorescence Lifetime Measurement. Fluorescence lifetimes for all the synthesized Ir(III) cyclometalated complexes were measured with the help of TCSPC (time-correlated single photon counting) equipped with a picosecond pulse diode laser excitation. A 20 μM solution of all the complexes was prepared in DMSO. Ir1@DEDTC, Ir1@MORDTC, and Ir1@MEDTC complexes were excited with an excitation pulse of 405 nm. The lifetime of Ir2@DEDTC and Ir2@MORDTC was measured with an excitation pulse of a 450 nm LED source. Average fluorescence lifetimes were calculated using the best-fitting model ($\chi^2 \sim 1$) with the help of the following formula for double exponential decay for Ir1@DEDTC, Ir1@MORDTC, and Ir1@MEDTC:

$$\overline{\tau} = \frac{A_1\tau_1^2 + A_2\tau_2^2}{A_1\tau_1 + A_2\tau_2}$$

4.5. Electron Paramagnetic Resonance (EPR). The EPR experiments were performed at room temperature (298 K) on a Bruker Biospin EMXmicro A200 spectrometer. Field modulation was given at 100 kHz and 0.05 mT, and the microwave attenuation was 0.657 mW with a microwave frequency of 9.410 GHz. The complexes were placed in a capillary positioned in a cavity. Irradiation was executed with a 450 nm blue LED light source. The following EPR parameters were used to acquire the spectra: sweep width of 5 mT, 1024 points, time constant of 40.96 ms, and conversion time of 150 ms, providing a sweep time of ∼150 s. The spin traps TEMP, DMPO, and BMPO (50 mM) were used to capture and identify the formation of different ROS produced by Ir2@DEDTC (100 μM) after irradiation with 450 nm light for 20 min.

4.6. Cell Viability Assay. The photocytotoxicity was measured in HeLa, HCT116, and PC3 cell lines. The cell viability assay was performed based on the previous light−dark experiment using 3-(4,5-dimethylthiazolyl-2)-2,5-diphenyltetrazolium bromide (MTT).[69] Briefly, 1 × 10^4 cells per well were seeded in two separate 96 well plates (dark and light plates, respectively) and grown for 24 h to acquire its morphology. The stock solution (5 mM) of synthesized iridium complexes was prepared in DMSO and further diluted with media (with FBS) so that the final concentration of DMSO in all of the wells was lower than 0.4%. Cells were further treated with different concentrations (2.5, 5, 10, and 20 μM) of complex and incubated for 24 h under dark conditions. After 24 h of incubation, 200 μL/well phosphate-buffered saline (PBS) was added to both plates after removing the previous media. The light plate was then irradiated with an LED source (456 nm, 30 mW/cm^2) for 40 min. Simultaneously the dark plate was kept in the dark with PBS for 40 min (without irradiation). After removing PBS, media (with FBS, 200 μL/well) is added in all wells and incubated for another 24 h. The cells were then washed further with PBS and incubated with a freshly prepared 10 μL (5 mg/mL) MTT in media (without FBS) for 4 h at 37 °C. After 4 h, 50 μL of media is removed carefully without disturbing the formazan crystal, and 150 μL of DMSO is added to each well. Using a microplate reader, the absorbance was measured at 570 nm and cell viability was calculated by comparing the absorbance of drug-treated cells with the untreated cells (cells alone). Cisplatin (FDA-approved drug) is used as a positive control. All data are based on three independent tests and are represented as the mean ± standard error (S.E.).

4.7. Detection and Quantification of Intracellular ROS. Intracellular ROS levels can be detected and measured by the fluorescent probe DCFH-DA. 5 ×10^4 HCT116 cells per well were seeded and grown in 6-well plates for 24 h. The cells were treated with 20 μM iridium complex and incubated for 4 h at 37 °C, 5% CO_2. Culture media was then removed, and 1 mL of PBS was added to each well. Cells were subjected to an LED light source (456 nm, 30 mW/cm^2) for 20 min. After that, cells were washed with 1× PBS and then incubated with DCFH-DA (20 μM) at 37 °C for 20 min under dark condition. Hydrogen peroxide (working conc 50 μM) was taken as a positive control. Cells were then washed with 1× PBS (1 mL) twice, and then images were captured in green channel and bright field with the help of an Olympus fluorescent inverted microscope. All of the images were taken at the same exposure time. After imaging, cells were trypsinized, collected, and centrifuged to make pellets that further dissolved in PBS. The fluorescence intensities were quantified by using a microplate reader with excitation (485 nm) and emission (535 nm), respectively. The obtained results were plotted as a fold

https://doi.org/10.1021/acs.inorgchem.3c02942
Inorg. Chem. 2023, 62, 20080−20095

increase in ROS generation correlated with the relative fluorescence of DCF compared to untreated cells under dark condition.

4.8. ICP-MS Analysis. The intracellular uptake of iridium complexes was determined by ICP-MS. Briefly, HCT116 cells were seeded to a density of approximately 1×10^5 cells per well in tissue culture 12-well plates. After 24 h, culture media was removed, and cells were treated with Ir2@DEDTC (20 μM) for different intervals, i.e., 2, 4, 6, and 12 h. After different incubation times with the complex, cells were washed (1 mL × 3) with PBS and trypsinized. Cells were collected by centrifugation and digested with 200 μL of HNO_3 (68%) for 24 h at room temperature. After 24 h of digestion in HNO_3, the solution was diluted to a final volume of 10 mL with distilled water or Milli-Q water. The concentration of Iridium was determined using Agilent 8900 ICP-MS Triple Quad.

4.9. DAPI Staining Assay. Approximately 6×10^4 HCT116 cells were seeded in six-well plates for 24 h and then further incubated with Ir2@DEDTC for 24 h. After light irradiation, cells are washed with 1× PBS and then fixed with 4% paraformaldehyde for 10 min. Cells were carefully washed again with 1× PBS and permeabilized by 0.1% TritonX100 for 10 min. After this, cells were washed again with 1× PBS and incubated with DAPI (1 μg/mL in PBS) for 30 min under dark conditions. After 30 min, cells were washed twice with 1× PBS, and images were captured with the help of a fluorescence microscope under a blue channel.

4.10. FDA/PI Costaining. First, a stock solution of FDA (5 mg/mL of acetone) and PI (1 mg/mL PBS) was prepared as per previous literature.[70] 5×10^4 cells were grown over the coverslip in a 6-well plate for 24 h. The cells were then treated with 20 μM Ir2@DEDTC for 6 and 24 h. After completion of the incubation time, the medium was replaced with PBS for the light group and irradiated for 20 min. Cells were carefully washed with 1× PBS and incubated with FDA (working concentration: 8 μg/mL) and PI (2 μg/mL) for 10 min in the dark. Then, cells were washed slowly with 1× PBS twice, and then coverslips were mounted over the slides to capture the images using an Olympus fluorescence microscope under bright field and green and red channels.

4.11. Fluorescence Imaging and Cellular Uptake. HCT116 cells (6×10^4 cells per well) were seeded in 6-well plates and grown over a coverslip for 24 h. The cells were then treated with iridium(III) complex and incubated for 8 h. After removing media, cells were carefully washed with 1× PBS and coverslips were mounted and images were obtained using an Olympus fluorescence microscope under bright light and red channel. The images reported were then further processed using ImageJ software.

4.12. Cellular Localization. Briefly, HCT116 cells (6×10^4 cells per well) were seeded in six-well plates and grown for 24 h. Cells were then incubated with Ir2@DEDTC (20 μM) for 6 h. After 6 h, cells were washed with 1× PBS and incubated with Mitotracker Green (500 nM), Lysotracker Green (500 nM), and DAPI (1 μg/mL), respectively, for 30 min in the dark. After this, cells were carefully washed with 1× PBS twice, and images were captured with the help of Olympus fluorescence microscope. The images were further processed with Fiji imageJ software and Pearson's R value is determined using Coloc2 plugin.

4.13. JC-1 Staining. HCT116 cells (5×10^4 cells per well) were seeded in 12-well plates and grown for 24 h. Cells were then incubated with Ir2@DEDTC (20 μM) for 6 h. After 6 h, the cells were washed with 1× PBS and incubated with JC-1 (5 μg/mL) for 30 min in the dark. After this, cells were carefully washed with 1× PBS twice, and images were captured with the help of an Olympus fluorescence microscope under bright field, green, and red channels with an exposure time of 394.4 ms.

4.14. Cell Cycle Arrest. HCT116 cells (6×10^4 cells per well) were seeded in 12 well plates and grown for 24 h. Cells were then incubated with Ir2@DEDTC (20 μM) for 24 h. After 24 h, the light plate is irradiated for 40 min (30 mW/cm^2) and then incubated for another 24 h. Cells were washed with 1× PBS and trypsinized to obtain the pellet. After this, all the pellets were carefully washed with ice-cold 1× PBS and further 70% ethanol was added dropwise while vortexing the pellets and incubated for 2 h at 4 °C to fix the cells. After this, RNA (100 μg/mL) and PI (50 μg/mL) were added, and flow cytometry was performed.

4.15. Spheroid Formation and Imaging. HCT116 cells (2×10^4 cells per well) were seeded in ultralow attachment 96-well plates (U-shaped wells) and grown for 72 h to get the desired spheroids. Spheroids were then incubated with Ir2@DEDTC (20 μM) for 24 h. Simultaneously, the light plate is irradiated for 40 min (30 mW/cm^2) and then incubated for another 24 h in drug free media. Spheroids were washed with 1× PBS, and further images were captured by an Olympus fluorescence inverted microscope under a bright channel for 6 days. Simultaneously, spheroids were stained with FDA/PI solution for 10 min in dark. Washing was done with 1× PBS two times, and then images were obtained in green and red channel.

■ ASSOCIATED CONTENT

Supporting Information

The Supporting Information is available free of charge at https://pubs.acs.org/doi/10.1021/acs.inorgchem.3c02942.

studies of UV−vis, NMR spectra, mass spectrometry data, crystallographic details with bond length and bond angles, emission spectra, lifetime data, DPBF absorption data, photostability analysis, EPR, uptake studies for iridium(III) complexes, and morphology changes in MCTS (PDF)

Accession Codes

CCDC 2277278 and 2277282 contain the supplementary crystallographic data for this paper. These data can be obtained free of charge via www.ccdc.cam.ac.uk/data_request/cif, or by emailing data_request@ccdc.cam.ac.uk, or by contacting The Cambridge Crystallographic Data Centre, 12 Union Road, Cambridge CB2 1EZ, UK; fax: +44 1223 336033.

■ AUTHOR INFORMATION

Corresponding Author

V. Venkatesh − *Department of Chemistry, Indian Institute of Technology Roorkee, Roorkee, Uttarakhand 247667, India;* orcid.org/0000-0001-9520-6842; Email: venkatesh.v@cy.iitr.ac.in

Authors

Monika Negi − *Department of Chemistry, Indian Institute of Technology Roorkee, Roorkee, Uttarakhand 247667, India*

Tejal Dixit − *Department of Chemistry, Indian Institute of Technology Roorkee, Roorkee, Uttarakhand 247667, India*

Complete contact information is available at: https://pubs.acs.org/10.1021/acs.inorgchem.3c02942

Author Contributions

V.V. and M.N. conceptualized the study. M.N. synthesized and characterized the complexes and performed all the biological studies. T.D. performed and analyzed the single crystal XRD analysis of the synthesized complexes. The manuscript was written through the contributions of all authors. All authors have approved the final version of the manuscript.

Notes

The authors declare no competing financial interest.

■ ACKNOWLEDGMENTS

V.V. sincerely acknowledges the Science and Engineering Research Board (CRG/2020/001398), New Delhi, India. The authors are thankful to Dr. B. V. V. S. Pavan Kumar for providing access to the fluorescence microscope facility. We are also grateful for Dr. Reena Kumari for her suggestions

while performing biological assays. We acknowledge the Institute Instrumentation Centre (IIC), IIT Roorkee for EPR, ICP-MS and FLS facilities, DST-FIST for NMR and single crystal XRD facility (SR/FST/CS-II/2018/72(C).

REFERENCES

(1) Sawant, S.; Shegokar, R. Cancer research and therapy: where are we today. *Int. J. Cancer Ther. Oncol.* **2014**, *2*, 020408.
(2) Imberti, C.; Zhang, P.; Huang, H.; Sadler, P. J. New Designs for Phototherapeutic Transition Metal Complexes. *Angew. Chem., Int. Ed.* **2020**, *59*, 61−73.
(3) Zhao, Z.; Gao, P.; Ma, L.; Chen, T. A highly X-ray sensitive iridium prodrug for visualized tumor radiochemotherapy. *Chem. Sci.* **2020**, *11*, 3780−3789.
(4) Heinemann, F.; Karges, J.; Gasser, G. Critical overview of the use of Ru(II) polypyridyl complexes as photosensitizers in one-photon and two-photon photodynamic therapy. *Acc. Chem. Res.* **2017**, *50*, 2727−2736.
(5) Xiao, Y.-F.; Chen, W.-C.; Chen, J.-X.; Lu, G.; Tian, S.; Cui, X.; Zhang, Z.; Chen, H.; Wan, Y.; Li, S.; Lee, C.-S. Amplifying Free Radical Generation of AIE Photosensitizer with Small Singlet−Triplet Splitting for Hypoxia-Overcoming Photodynamic Therapy. *ACS Appl. Mater. Interfaces* **2022**, *14*, 5112−5121.
(6) Huang, X.; Zhang, W.; Peng, Y.; Gao, L.; Wang, F.; Wang, L.; Wei, X. A Multifunctional Layered Nickel Silicate Nanogenerator of Synchronous Oxygen Self-Supply and Superoxide Radical Generation for Hypoxic Tumor Therapy. *ACS Nano* **2022**, *16*, 974−983.
(7) Perillo, B.; Di Donato, M.; Pezone, A.; Di Zazzo, E.; Giovannelli, P.; Galasso, G.; Castoria, G.; Migliaccio, A. ROS in cancer therapy: the bright side of the moon. *Exp Mol. Med.* **2020**, *52*, 192−203.
(8) Wang, K.; Ye, T.; Du, H.; Jin, X.; Yi, X.; Gao, H.; Zhang, Y.; Dong, W.; Liu, S.; Guan, J.; Lin, F.; Xia, D. Synthesis and properties of novel type I photosensitizer polycyclic amide. *Nanoscale Adv.* **2023**, *5*, 3629−3633.
(9) Xie, S.; Cong, Z.; Wang, W.; Qin, S.; Weng, X.; Song, H.; Zhou, X. Mitochondria-targeting NIR AIEgens with cationic amphiphilic character for imaging and efficient photodynamic therapy. *Chem. Commun.* **2023**, *59*, 2592−2595.
(10) Yang, K.; Zhou, Y.; Wang, Y.; Zhao, S.; Wu, X.; Peng, X.; Huang, L.; Jiang, L.; Lan, M.; Yi, X. Y. An Iridium Complex as an AIE-active Photosensitizer for Image-guided Photodynamic Therapy. *Chem. - Asian J.* **2021**, *16*, 1780−1785.
(11) Xu, Y.; Wang, X.; Song, K.; Du, J.; Liu, J.; Miao, Y.; Li, Y. BSA-encapsulated cyclometalated iridium complexes as nano-photosensitizers for photodynamic therapy of tumor cells. *RSC Adv.* **2021**, *11*, 15323−15331.
(12) Wu, N.; Cao, J.-J.; Wu, X.-W.; Tan, C.-P.; Ji, L.-N.; Mao, Z.-W. Iridium(III) complexes with five-membered heterocyclic ligands for combined photodynamic therapy and photoactivated chemotherapy. *Dalton Trans.* **2017**, *46*, 13482−13491.
(13) Zheng, Y.; He, L.; Zhang, D.-Y; Tan, C.-P.; Ji, L.-N.; Mao, Z.-W. Mixed-ligand iridium(iii) complexes as photodynamic anticancer agents. *Dalton Trans.* **2017**, *46*, 11395−11407.
(14) Zamora, A.; Vigueras, G.; Rodríguez, V.; Santana, M. D.; Ruiz, J. Cyclometalated Iridium(III) Luminescent Complexes in Therapy and Phototherapy. *Coord. Chem. Rev.* **2018**, *360*, 34−76.
(15) Tong, J.; Yang, X.; Song, X.; Liang, J.; Huang, S.; Mao, H.; Akhtar, M.; Liu, A.; Shan, G.-G.; Li, G. AIE-active Ir(iii) complexes as type-I dominant photosensitizers for efficient photodynamic therapy. *Dalton Trans.* **2023**, *52*, 1105−1112.
(16) Kuang, S.; Wei, F.; Karges, J.; Ke, L.; Xiong, K.; Liao, X.; Gasser, G.; Ji, L.; Chao, H. Photodecaging of mitochondria-Localized Iridium(III) Endoperoxide Complex for two-photon photoactivated therapy under Hypoxia. *J. Am. Chem. Soc.* **2022**, *144*, 4091−4101.
(17) Zhao, J.; Sun, S.; Li, X.; Zhang, W.; Gou, S. Enhancing Photodynamic Therapy Efficacy of Upconversion-Based Nanoparticles Conjugated with a Long-Lived Triplet Excited State Iridium(III)-Naphthalimide Complex: Toward Highly Enhanced Hypoxia-Inducible Factor-1. *ACS Appl. Bio Mater.* **2020**, *3*, 252−262.
(18) Fan, Z.; Rong, Y.; Sadhukhan, T.; Liang, S.; Li, W.; Yuan, Z.; Zhu, Z.; Guo, S.; Ji, S.; Wang, J. Single-Cell Quantification of a Highly Biocompatible Dinuclear Iridium(III) Complex for Photocatalytic Cancer Therapy. *Angew. Chem., Int. Ed.* **2022**, *61*, e202202098.
(19) Huang, H.; Banerjee, S.; Sadler, P. J. Recent advances in the design of targeted iridium(III) photosensitizers for photodynamic therapy. *ChemBioChem.* **2018**, *19*, 1574−1589.
(20) Yang, Y.; Guo, L.; Tian, Z.; Gong, Y.; Zheng, H.; Zhang, S.; Xu, Z.; Ge, X.; Liu, Z. Novel and Versatile Imine-N-Heterocyclic Carbene Half-Sandwich Iridium(III) Complexes as Lysosome-Targeted Anticancer Agents. *Inorg. Chem.* **2018**, *57*, 11087−11098.
(21) Li, Y.; Liu, Bi.; Lu, X.-R.; Li, M.-F.; Ji, L.-N.; Mao, Z.-W. Cyclometalated iridium(III) N-heterocyclic carbene complexes as potential mitochondrial anticancer and photodynamic agents. *Dalton Trans.* **2017**, *46*, 11363−11371.
(22) Zhong, M.; He, J.; Zhang, B.; Liu, Q.; Fang, J. Mitochondria-targeted iridium-based photosensitizers enhancing photodynamic therapy effect by disturbing cellular redox balance. *Free Radic. Biol. Med.* **2023**, *195*, 121−131.
(23) Ye, R.-R; Tan, C.-P.; Ji, L.-N.; Mao, Z.-W. Coumarin-appended phosphorescent cyclometalated iridium(III) complexes as mitochondria-targeted theranostic anticancer agents. *Dalton Trans.* **2016**, *45*, 13042−13051.
(24) Xiang, H.; Chen, H.; Tham, H. P.; Phua, S. Z. F.; Liu, J.-G.; Zhao, Y. Cyclometalated iridium (III)-complex-based micelles for glutathione-responsive targeted chemotherapy and photodynamic therapy. *ACS Appl. Mater. Interfaces* **2017**, *9*, 27553−27562.
(25) Hu, C.; Xu, S.; Song, Z.; Li, H.; Liu, H. Recent Advance in Nucleus-Targeted Fluorescent Probes for Bioimaging, Detection, and Therapy. *Chemosensors* **2023**, *11*, 125.
(26) Zhang, P.; Huang, H.; Banerjee, S.; Clarkson, G. J.; Ge, C.; Imberti, C.; Sadler, P. J. Nucleus-Targeted Organoiridium−Albumin Conjugate for Photodynamic Cancer Therapy. *Angew. Chem., Int. Ed.* **2019**, *58*, 2350−2354.
(27) Nam, J. S.; Kang, M.-G.; Kang, J.; Park, S.-Y.; Lee, S. J. C.; Kim, H.-T.; Seo, J. K.; Kwon, O.-H.; Lim, M. H.; Rhee, H.-W.; Kwon, T.-H. Endoplasmic Reticulum-Localized Iridium(III) Complexes as Efficient Photodynamic Therapy Agents via Protein Modifications. *J. Am. Chem. Soc.* **2016**, *138*, 10968−10977.
(28) Wang, L.; Guan, R.; Xie, L.; Liao, X.; Xiong, K.; Rees, T. W.; Chen, Y.; Ji, L.; Chao, H. An ER-targeting iridium(III) complex that induces immunogenic cell death in non-small-cell lung cancer. *Angew. Chem., Int. Ed.* **2021**, *60*, 4657−4665.
(29) Kuang, S.; Liao, X.; Zhang, X.; Rees, T. W.; Guan, R.; Xiong, K.; Chen, Y.; Ji, L.; Chao, H. FerriIridium: A Lysosome-Targeting Iron(III)-Activated Iridium(III) Prodrug for Chemotherapy in Gastric Cancer Cells. *Angew. Chem., Int. Ed.* **2020**, *59*, 3315−3321.
(30) Wang, K.-N.; Liu, L.-Y.; Qi, G.; Chao, X.-J.; Ma, W.; Yu, Z.; Pan, Q.; Mao, Z.-W.; Liu, B. Light-driven cascade mitochondria to nucleus photosensitization in cancer cell ablation. *Adv. Sci.* **2021**, *8*, 2004379.
(31) Katlenok, E. A.; Rozhkov, A. V.; Ramazanov, R. R.; Valiev, R. R.; Levin, O. V.; Goryachiy, D. O.; Taydakov, I. V.; Kuznetsov, M. L.; Kukushkin, V. Y. Photo and Electroluminescent Neutral Iridium(III) Complexes Bearing Imidoylamidinate Ligands. *Inorg. Chem.* **2022**, *61*, 8670−8684.
(32) Bin Mohd Yusoff, A. R.; Huckaba, A. J.; Nazeeruddin, M. K. Phosphorescent neutral iridium (III) complexes for organic light-emitting diodes. *Top. Curr. Chem.* **2017**, *375*, 39.
(33) Wang, X.; Song, K.; Deng, Y.; Liu, J.; Peng, Q.; Lao, X.; Xu, J.; Wang, D.; Shi, T.; Li, Y.; Deng, D.; Miao, Y. Benzothiazole-decorated iridium-based nanophotosensitizers for photodynamic therapy of cancer cells. *Dalton Trans.* **2022**, *51*, 3666−3675.
(34) Pan, Z.-Y.; Feng, W.-W.; Liu, Q.-Y.; He, L.; Yao, D.-H.; He, Z.-D. Lipophilic neutral iridium(III) complexes for phosphorescence imaging of lipid droplets and potential photodynamic therapy. *Dyes Pigm.* **2022**, *203*, 110387.

https://doi.org/10.1021/acs.inorgchem.3c02942
Inorg. Chem. 2023, 62, 20080−20095

(35) Huang, T.; Yu, Q.; Liu, S.; Zhang, K. Y.; Huang, W.; Zhao, Q. Rational Design of Phosphorescent Iridium(III) Complexes for Selective Glutathione Sensing and Amplified Photodynamic Therapy. *ChemBioChem.* **2019**, *20*, 576−586.
(36) Wu, Y.; Liu, J.; Shao, M.; Zhang, P.; Song, S.; Yang, G.; Liu, X.; Liu, Z. Cyclometalated iridium(III) dithioformic acid complexes as mitochondria-targeted imaging and anticancer agents. *J. Inorg. Biochem.* **2022**, *233*, 111855.
(37) Liu, J.-B.; Wu, C.; Chen, F.; Leung, C.-H.; Ma, D.-L. A simple iridium(III) dimer as a switch-on luminescent chemosensor for carbon disulfide detection in water samples. *Anal. Chim. Acta* **2019**, *1083*, 166−171.
(38) Mei, Q.-b.; Guo, Y.-h.; Tong, B.-h.; Weng, J.-N.; Zhang, B.; Huang, W. Phosphorescent chemosensor for Hg^{2+} and acetonitrile based on iridium(III) complex. *Analyst* **2012**, *137*, 5398−5402.
(39) Mei, Q.; Shi, Y.; Hua, Q.; Tong, B. Phosphorescent chemosensor for Hg^{2+} based on an iridium(III) complex coordinated with 4-phenylquinazoline and carbazole dithiocarbamate. *RSC Adv.* **2015**, *5*, 74924−74931.
(40) Lu, G.-Z.; Su, N.; Yang, H.-Q.; Zhu, Q.; Zhang, W.-W.; Zheng, Y.-X.; Zhou, L.; Zuo, J.-L.; Chen, Z.-X.; Zhang, H.-J. Rapid room temperature synthesis of red iridium(III) complexes containing a four-membered Ir−S−C−S chelating ring for highly efficient OLEDs with EQE over 30%. *Chem. Sci.* **2019**, *10*, 3535−3542.
(41) Su, N.; Li, F.-L.; Zheng, Y.-X. Four-membered red iridium(III) complexes with Ir−S−C−S structures for efficient organic light-emitting diodes. *J. Mater. Chem. C* **2020**, *8*, 7411−7416.
(42) Mei, Q.; Chen, C.; Tian, R.; Yang, M.; Tong, B.; Hua, Q.; Shi, Y.; Fan, Q.; Ye, S. Highly efficient orange phosphorescent organic light-emitting diodes based on an iridium(III) complex with diethyldithiocarbamate (S^S) as the ancillary ligand. *RSC Adv.* **2016**, *6*, 64003−64008.
(43) Mukherjee, T.; Mukherjee, M.; Sen, B.; Banerjee, S.; Hundal, G.; Chattopadhyay, P. Synthesis, characterization, interaction with DNA and bovine serum albumin (BSA), and antibacterial activity of cyclometalated iridium(III) complexes containing dithiocarbamate derivatives. *J. Coord. Chem.* **2014**, *67*, 2643−2660.
(44) Lin, C.; Wang, X.; Nao, S.-C.; Wang, J.; Liu, J.; Ma, D.-L.; Zhu, W.-G.; Leung, C.-H.; Wang, W. A labile iridium(III) complex-based luminogenic probe for the ratiometric detection of dithiocarbamate compounds in living system. *Sens. Actuators, B* **2023**, *378*, 133133.
(45) Nguyen, V.-N.; Qi, S.; Kim, S.; Kwon, N.; Kim, G.; Yim, Y.; Park, S.; Yoon, J. An Emerging Molecular Design Approach to Heavy-Atom-Free Photosensitizers for Enhanced Photodynamic Therapy under Hypoxia. *J. Am. Chem. Soc.* **2019**, *141*, 16243−16248.
(46) Lai, P.-N.; Yoon, S.; Wu, Y.; Teets, T. S. Effects of Ancillary Ligands on Deep Red to Near-Infrared Cyclometalated Iridium Complexes. *ACS Org. Inorg. Au* **2022**, *2*, 236−244.
(47) Nguyen, V.-N.; Baek, G.; Qi, S.; Heo, S.; Yim, Y.; Yoon, J. A lysosome-localized thionaphthalimide as a potential heavy-atom-free photosensitizer for selective photodynamic therapy. *Dyes Pigm.* **2020**, *177*, 108265.
(48) Sumit; Maravajjala, K. S.; Khanna, S.; Kachwal, V.; Swetha, K. L.; Manabala, S.; Chowdhury, R.; Roy, A.; Laskar, I. R. Rational Molecular Designing of Aggregation-Enhanced Emission (AEE) Active Red-Emitting Iridium(III) Complexes: Effect of Lipophilicity and Nanoparticle Encapsulation on Photodynamic Therapy Efficacy. *ACS Appl. Bio Mater.* **2023**, *6*, 1445−1459.
(49) Prajapati, M. J.; Solanki, J. D.; Machhi, H. K.; Soni, S. S.; Sen, P.; Surati, K. R. Yellowish-orange phosphorescent iridium(III) complexes of bis-cyclometalated ligand with pyrazolone derivatives: synthesis, characterization, photophysical and thermal properties. *J. Mater. Sci: Mater. Electron* **2020**, *31*, 13778−13786.
(50) Yi, S.; Kim, J.-H.; Cho, Y.-J.; Lee, J.; Choi, T.-S.; Cho, D. W.; Pac, C.; Han, W.-S.; Son, H.-J.; Kang, S. O. Stable Blue Phosphorescence Iridium(III) Cyclometalated Complexes Prompted by Intramolecular Hydrogen Bond in Ancillary Ligand. *Inorg. Chem.* **2016**, *55*, 3324−3331.
(51) Lamansky, S.; Djurovich, P.; Murphy, D.; Abdel-Razzaq, F.; Lee, H.-E.; Adachi, C.; Burrows, P. E.; Forrest, S. R.; Thompson, M. E. Highly Phosphorescent Bis-Cyclometalated Iridium Complexes: Synthesis, Photophysical Characterization, and Use in Organic Light Emitting Diodes. *J. Am. Chem. Soc.* **2001**, *123*, 4304−4312.
(52) Takizawa, S.; Aboshi, R.; Murata, S. Photooxidation of 1,5-dihydroxynaphthalene with iridium complexes as singlet oxygen sensitizers. *Photochem. Photobiol. Sci.* **2011**, *10*, 895−903.
(53) Sun, J.; Wu, W.; Guo, H.; Zhao, J. Visible-Light Harvesting with Cyclometalated Iridium(III) Complexes Having Long-Lived ^{3}IL Excited States and Their Application in Triplet-Triplet-Annihilation Based Upconversion. *Eur. J. Inorg. Chem.* **2011**, *2011*, 201190060.
(54) Liu, B.; Monro, S.; Li, Z.; Jabed, M. A.; Ramirez, D.; Cameron, C. G.; Colón, K.; Roque, J., III; Kilina, S.; Tian, J.; McFarland, S. A.; Sun, W. A New Class of Homoleptic and Heteroleptic Bis-(terpyridine) Iridium(III) Complexes with Strong Photodynamic Therapy Effects. *ACS Appl. Bio Mater.* **2019**, *2*, 2964−2977.
(55) Monro, S.; Colón, K. L.; Yin, H.; Roque, J.; Konda, P.; Gujar, S.; Thummel, R. P.; Lilge, L.; Cameron, C. G.; McFarland, S. A. Transition Metal Complexes and Photodynamic Therapy from a Tumor-Centered Approach: Challenges, Opportunities, and Highlights from the Development of TLD1433. *Chem. Rev.* **2019**, *119*, 797−828.
(56) Wu, C.; Li, Q.; Zhang, X.; Shi, C.; Li, G.; Wang, M.; Li, K.; Yuan, A. Tuning the Photophysical and Excited State Properties of Phosphorescent Iridium(III) Complexes by Polycyclic Unit Substitution. *Chem. Open* **2019**, *8*, 339−343.
(57) Hua, T.; Zhan, L.; Li, N.; Huang, Z.; Cao, X.; Xiao, Z.; Gong, S.; Zhou, C.; Zhong, C.; Yang, C. Heavy-atom effect promotes multi-resonance thermally activated delayed fluorescence. *Chem. Eng. J.* **2021**, *426*, 131169.
(58) Martínez-Fernández, L.; Corral, I.; Granucci, G.; Persico, M. Competing Ultrafast Intersystem Crossing and Internal Conversion: a Time Resolved Picture for the Deactivation of 6-Thioguanine. *Chem. Sci.* **2014**, *5*, 1336−1347.
(59) Pollum, M.; Jockusch, S.; Crespo-Hernández, C. E. 2,4-Dithiothymine as a Potent UVA Chemotherapeutic Agent. *J. Am. Chem. Soc.* **2014**, *136*, 17930−17933.
(60) Tang, T. S.-M.; Leung, K.-K.; Louie, M.-W.; Liu, H.-W.; Cheng, S. H.; Lo, K. K.-W. Phosphorescent biscyclometallated iridium(III) ethylenediamine complexes functionalised with polar ester or carboxylate groups as bioimaging and visualisation reagents. *Dalton Trans.* **2015**, *44*, 4945−4956.
(61) Zhang, P.; Chiu, C. K. C.; Huang, H.; Lam, Y. P. Y.; Habtemariam, A.; Malcomson, T.; Paterson, M. J.; Clarkson, G. J.; O'Connor, P. B.; Chao, H.; Sadler, P. J. Organoiridium Photosensitizers Induce Specific Oxidative Attack on Proteins within Cancer Cells. *Angew. Chem., Int. Ed.* **2017**, *56*, 14898−14902.
(62) Jones, K.; Kim, D. W.; Park, J. S.; Khang, C. H. Live-cell fluorescence imaging to investigate the dynamics of plant cell death during infection by the rice blast fungus Magnaporthe oryzae. *BMC Plant Biol.* **2016**, *16*, 69.
(63) Gupta, A.; Pandey, A. K.; Mondal, T.; Bhattacharya, J.; Sasmal, P. K. Multifunctional Iridium(III)−Platinum(IV) Conjugates as Potent Anticancer Theranostic Agents. *J. Med. Chem.* **2023**, *66*, 8687−8704.
(64) Sarma, M.; Chatterjee, T.; Bodapati, R.; Krishnakanth, K. N.; Hamad, S.; Venugopal Rao, S.; Das, S. K. Cyclometalated Iridium(III) Complexes Containing 4,4′-π-Conjugated 2,2′-Bipyridine Derivatives as the Ancillary Ligands: Synthesis, Photophysics, and Computational Studies. *Inorg. Chem.* **2016**, *55*, 3530−3540.
(65) Brustolin, L.; Nardon, C.; Pettenuzzo, N.; Zuin Fantoni, N.; Quarta, S.; Chiara, F.; Gambalunga, A.; Trevisan, A.; Marchiò, L.; Pontisso, P.; Fregona, D. Synthesis, chemical characterization and cancer cell growth-inhibitory activities of Cu(II) and Ru(III) aliphatic and aromatic dithiocarbamato complexes. *Dalton Trans.* **2018**, *47*, 15477−15486.
(66) Bevernaegie, R.; Wehlin, S. A. M.; Elias, B.; Troian-Gautier, L. A Roadmap Towards Visible Light Mediated Electron Transfer

Chemistry with Iridium(III) Complexes. *ChemPhotoChem.* **2021**, *5*, 217−234.
(67) Liao, X.; Shen, J.; Wu, W.; Kuang, S.; Lin, M.; Karges, J.; Tang, Z.; Chao, H. A mitochondrial-targeting iridium(iii) complex for H_2O_2-responsive and oxidative stress amplified two-photon photodynamic therapy. *Inorg. Chem. Front.* **2021**, *8*, 5045−5053.
(68) Li, Y.; Tan, C.-P.; Zhang, W.; He, L.; Ji, L.-N.; Mao, Z.-W. Phosphorescent iridium(III)-bis-N-heterocyclic carbene complexes as mitochondria-targeted theranostic and photodynamic anticancer agents. *Biomaterials* **2015**, *39*, 95−104.
(69) Ouyang, M.; Zeng, L.; Qiu, K.; Chen, Y.; Ji, L.; Chao, H. Cyclometalated Ir^{III} Complexes as Mitochondria-Targeted Photodynamic Anticancer Agents. *Eur. J. Inorg. Chem.* **2017**, 1764−1771.
(70) Metzger, K.; Dannenberger, D.; Tuchscherer, A.; Ponsuksili, S.; Kalbe, C. Effects of temperature on proliferation of myoblasts from donor piglets with different thermoregulatory maturities. *BMC Mol. and Cell Biol.* **2021**, *22*, 36.

https://doi.org/10.1021/acs.inorgchem.3c02942
Inorg. Chem. 2023, 62, 20080−20095